

# Paving the Way for Scientific Foundation Models: Enhancing Generalization and Robustness in PDEs with Constraint-Aware Pre-Training

Amin Totounferoush\*

University of Stuttgart, Germany

Michael W. Mahoney

ICSI, LBNL, and

University of California, Berkeley, USA

Serge Kotchourko\*

University of Stuttgart, Germany

Steffen Staab

University of Stuttgart, Germany

## Abstract

Partial differential equations (PDEs) govern a wide range of physical systems, but solving them efficiently remains a major challenge. The idea of a scientific foundation model (SciFM) is emerging as a promising tool for learning transferable representations across diverse domains. However, SciFMs require large amounts of solution data, which may be scarce or computationally expensive to generate. To maximize generalization while reducing data dependence, we propose incorporating PDE residuals into pre-training—either as the sole learning signal or in combination with data loss—to compensate for limited or infeasible training data. We evaluate this constraint-aware pre-training across three key benchmarks: (i) generalization to new physics, where material properties, e.g., the diffusion coefficient, is shifted with respect to the training distribution; (ii) generalization to entirely new PDEs, requiring adaptation to different operators; and (iii) robustness against noisy fine-tuning data, ensuring stability in real-world applications. Our results show that pre-training with PDE constraints significantly enhances generalization, outperforming models trained solely on solution data across all benchmarks. These findings prove the effectiveness of our proposed constraint-aware pre-training as a crucial component for SciFMs, providing a scalable approach to data-efficient, generalizable PDE solvers. The code used in this work is publicly-available.<sup>1</sup>

## 1 Introduction

Foundation models have revolutionized fields such as computer vision (CV) [4, 17] and natural language processing (NLP) [2, 1, 18], enabling advancements in generalization, adaptability, and efficiency across a wide range of tasks. These models leverage large-scale data and pre-training strategies to learn representations that can be fine-tuned with minimal effort for various downstream applications. Building on these successes, there is growing interest in developing scientific foundation models (SciFMs) to address complex physical and engineering problems. Scientific machine learning (SciML) leverages machine learning to solve complex scientific and engineering problems, particularly those governed by partial differential equations (PDEs). PDEs model diverse physical phenomena, but traditional numerical solvers, such as finite difference [5] and finite element [31] methods, are computationally expensive and scale poorly with (physics) complexity. They also require expert knowledge and fine-tuned parameters, limiting their adaptability. This highlights the need for faster, more generalizable approaches that can efficiently solve PDEs across different settings with minimal manual intervention.

Machine learning presents a promising pathway to overcome the challenges of traditional PDE solvers by offering faster, data-driven alternatives. Conventional approaches, such as physics-informed neural networks (PINNs) [9, 20], try to incorporate physical constraints into the learning process to enhance interpretability and ensure compliance with governing equations. While sometimes effective, these models are brittle [11], and they often struggle to generalize beyond their training data, limiting their adaptability to new parameter distributions or entirely different PDE types, without extensive retraining. More recent advancements, such as neural operators [10]—particularly Fourier neural operators (FNOs) [12]—have

\*equal contribution

<sup>1</sup><https://github.com/kotserge/physics-aware-sfm>

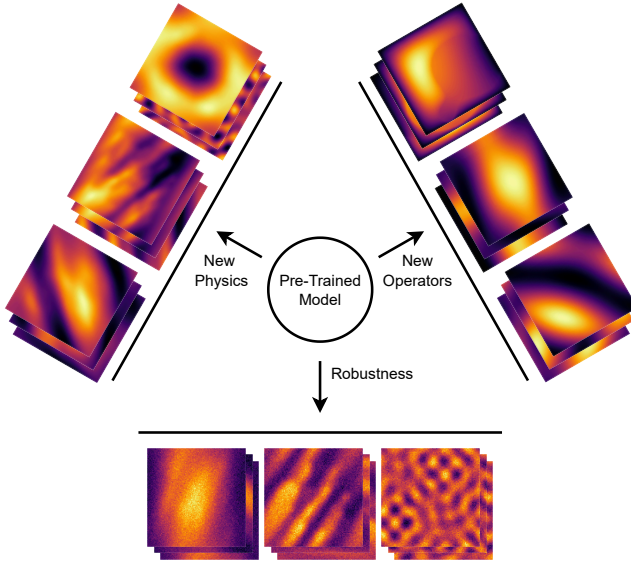


Figure 1: We explore the generalization abilities of constraint-aware pre-trained scientific models across a range of problem settings, investigating the models’ capacity to adapt to unseen parameter distributions (new physics), as well as to PDEs that were not seen in the pre-training (new operators). Further, we assess the models’ resilience to noisy fine-tuning data (Robustness), which is frequently encountered in real-world applications.

improved the generalization capabilities of SciML by learning solution operators rather than specific PDE instances. These methods aim to capture mappings between function spaces, allowing for better adaptability across varying PDE parameters. However, despite their flexibility, neural operators are restricted to the PDE operators on which they are trained, and they struggle to generalize to entirely new ones without fine-tuning. For example, a model trained on the Laplace operator does not generalize effectively to the curl operator. SciFMs have the potential to generalize across multiple PDE operators, including those encountered during pre-training and entirely new ones. These models are typically pre-trained on large, diverse PDE solution datasets and later adapted to specific tasks through fine-tuning [22] or in-context learning [30].

**A key limitation** of current SciFMs is their heavy reliance on PDE solution data. To develop a SciFM capable of generalizing across multiple PDE operators, one would need to construct an extensive dataset of solution data covering a wide range of operators and a broad distribution of PDE parameters, such as diffusion coefficients. This requirement arises because each PDE operator exhibits distinct mathematical characteristics, and small variations in PDE parameters can significantly alter solution behavior. Unlike tasks in CV or NLP, where minor changes in input may have limited impact, even slight parameter shifts in PDEs can drastically affect stability and solution structure. For instance, increasing the advection-to-diffusion coefficient ratio in an advection-diffusion equation (see Appendix A) can lead to severe numerical instability. Thus, an effective SciFM would require a vast and diverse dataset spanning multiple PDEs with a large coefficient range, which is computationally expensive, potentially infeasible, and may not account for unknown operators. This highlights the limitations of SciFMs that are trained only on numerical solution data, at least with current constraints.

We propose incorporating PDE residuals into the pre-training process to compensate for missing solution data. Specifically, we leverage PDE residuals in the training loss, which allows the model to learn PDE representations without explicit solution data, thereby enriching its generalization capabilities. Conceptually, this can be implemented in two ways:

- Pre-training solely with PDE residuals, covering a wide range of PDEs without requiring solution data.
- Combining PDE residuals with data loss to investigate the trade-offs and potential improvements in generalization.

We investigate both approaches in this paper, using six fundamental PDE systems essential to scientific and engineering applications. Pre-training is conducted on three steady-state PDEs: Poisson, Advection-Diffusion, and Helmholtz equations. For evaluation, we extend to three time-dependent initial value problems: Reaction-Diffusion, Advection-Reaction-Diffusion, and Darcy equations.

**Contributions and Scope of Investigation.** We assess whether constraint-aware pre-training can effectively mitigate data scarcity in the development of SciFMs. We employ the FNO due to its computational efficiency and ability to learn mappings between function spaces. We evaluate the performance of constraint-aware pre-trained models across the following key challenges, visualized in Figure 1:

1. **Generalization to new physics.** We evaluate the model’s ability to generalize within the same PDE operator under shifted PDE parameters. For instance, we pre-train the model with a diffusion coefficient sampled from  $D \sim (1, 5)$  and fine-tune it with  $D \sim (12, 15)$ . This shift introduces significantly different behavior (physics) compared to the pre-training data.
2. **Generalization to new operators.** We assess the model’s ability to generalize beyond pre-trained PDE operators to entirely new ones, i.e., given operators  $\mathcal{G}_1, \mathcal{G}_2, \dots, \mathcal{G}_n$  during pre-training, we evaluate performance on unseen operators  $\mathcal{G}_{\text{new-1}}, \mathcal{G}_{\text{new-2}}, \dots$ . Additionally, we examine whether a model trained on steady-state PDEs with periodic boundary conditions can generalize to time-dependent PDEs with different boundary conditions, such as Dirichlet or Neumann. This helps evaluate constraint-aware pre-trained models’ ability to transition from simpler steady-state problems to more complex, dynamic settings.
3. **Robustness to noisy fine-tuning data.** In practical scenarios, fine-tuning data is often corrupted by noise. We analyze the robustness of the pre-trained foundation model when fine-tuned with noisy data. Our goal is to determine the extent to which constraint-aware learning aids in mitigating the impact of noise and enhances model robustness.

Through these investigations, we aim to answer our original question: Can constraint-aware pre-trained models mitigate the challenges of data scarcity and computational expense in developing SciFMs? Our findings will provide insights into their effectiveness, limitations, and potential areas for improvement.

## 2 Related Works

There has been significant progress in leveraging machine learning methods to solve PDEs, with a focus on PINNs [20, 9, 11, 27, 16, 26] and neural operator-based approaches such as FNOs [12, 13] and DeepONets [14, 6]. PINNs try to enforce physical consistency through loss constraints, but they struggle with generalization to new parameters or PDE types. In contrast, neural operators learn mappings between function spaces, offering greater flexibility and scalability [12]. Despite these advancements, neural operators exhibit limited generalization, struggling to extend beyond the PDE operators on which they were trained.

Transfer learning has emerged as a promising approach to address these limitations, enabling models to adapt to new problems with reduced computational overhead. Previous studies have explored transfer learning between different geometries, resolutions and scales [29, 28, 25, 21, 8] demonstrating the ability of these models to generalize under specific conditions. However, these studies focus solely on within-distribution tasks and do not explore generalization to unseen PDE systems or boundary conditions. Additionally, the impact of fine-tuning data noise on performance remains unexplored.

Recent work has explored in-context learning for PDEs [30, 3], where transformer-based models leverage demonstrations (demos) provided within the prompt to solve differential equations. These models map input queries to correct solutions by mimicking the examples in the prompt, enabling them to address tasks similar to those seen in the demos. While promising, this approach heavily relies on the quality and diversity of the training demos, and its ability to generalize to new problem settings, such as unseen PDEs, remains a significant challenge.

Another line of research focuses on pre-training and fine-tuning strategies, as explored in [22, 15, 19, 7]. The work most closely related to ours is [22], which investigates transfer learning across PDE operators within a pre-training and fine-tuning framework. Their study examines factors such as the impact of fine-tuning dataset size, model scale, and generalization to the same PDE with different parameter distributions, as well as to entirely new PDE types.

These works demonstrate the effectiveness of pre-training and fine-tuning. However, as discussed in Sec. 1, they all rely on solution data for pre-training, limiting their feasibility to build a larger models. Building a SciFM requires a broader representation of problems, which is infeasible if reliant solely on solution data due to the diversity of PDEs and the high cost of data acquisition. To address this, we propose constraint-aware pre-training as a data-efficient approach, enabling the model to learn representations without explicit solution data. We show that this method generalizes better to unseen PDE operators, transfers from simpler problems (steady-state) to more challenging problems (time-dependent), and generalizes well to new problem settings even when fine-tuning data is noisy. These findings answer our research question and pave the way for developing SciFMs with broader and more scalable representations.

### 3 Methodology

We aim to approximate the solution of PDEs using machine learning techniques. Mathematically, a general form of a PDE can be expressed as:

$$\mathcal{G}(u; \lambda) = f(\mathbf{x}, \mathbf{t}), \quad \mathbf{x} \in \Omega, \quad \mathbf{t} \in \tau, \quad (1)$$

where  $\mathcal{G}$  is a differential operator (e.g., Laplace, Poisson, or Navier-Stokes operator),  $u(\mathbf{x})$  is the unknown solution we seek to approximate,  $\lambda$  represents the PDE parameters such as material properties,  $f(\mathbf{x}, \mathbf{t})$  is the force function,  $\Omega$  is the spatial domain, and  $\tau$  is the time domain.

Our objective is to learn a machine learning model  $\mathcal{F}_\theta$  that approximates the solution  $u(\mathbf{x}, \mathbf{t})$  by mapping the force function, initial condition, and PDE parameters to the solution:

$$\mathcal{F}_\theta(f, \lambda) \approx u(\mathbf{x}, \mathbf{t}). \quad (2)$$

where  $\theta$  describes the model’s parameters<sup>2</sup>.

We employ a two-stage learning strategy: pre-training and fine-tuning. Our approach involves generating a diverse dataset of solutions corresponding to various PDEs with different parameter distributions. The model is first pre-trained on a subset of these PDEs to learn general representations of the solution space. Subsequently, we fine-tune the foundation model on specific downstream tasks, and we perform investigations explained in Sec. 1 to assess the effectiveness of the proposed approach.

#### 3.1 Training and Evaluation PDE Systems Setup

We consider six fundamental PDE systems that serve as building blocks for various scientific and engineering applications. We use three steady-state PDEs for pre-training: Poisson, Advection-Diffusion, and Helmholtz equations. For evaluation, we extend this set to include three time-dependent initial value problems: Reaction-Diffusion, Advection-Reaction-Diffusion, and Darcy equations. Each system is defined over the spatial domain  $\Omega = [0, 1]^2$ , with time-dependent problems evolving over  $\tau = [0, 1]$ . Except for Darcy, which employs Dirichlet boundary condition, all PDEs assume periodic boundary conditions. The steady-state problems aim to map the force function and PDE parameters to the steady-state solution. In contrast, the time-dependent problems map the PDE parameters and initial condition to the solution at  $t = 1$  in this study. For further details, see Appendix A.

#### 3.2 Pre-training Strategies

To develop a data-efficient model for solving PDEs, we employ two distinct pre-training strategies aimed at capturing both the physical constraints and data-driven patterns. These strategies are: pre-training via PDE residuals; and pre-training via data-driven losses and PDE constraints.

##### 3.2.1 Pre-training via PDE residuals

In this approach, the model is trained solely using the PDE residuals, ensuring that the learned solution satisfies the governing physical laws. Given a general steady-state PDE, the physics-based loss function is formulated as:

---

<sup>2</sup>Note that in this work, all model inputs—such as the force function, initial conditions, and PDE parameters—as well as the outputs (solutions) are discrete representations of the underlying continuous functions.

$$\mathcal{L}_{\text{PDE}}(\theta) = \frac{1}{N} \sum_{i=1}^N \|\mathcal{G}(\mathcal{F}_\theta(f_i, \lambda_i)) - f_i\|^2, \quad (3)$$

where  $\mathcal{F}_\theta$  is the neural network parameterized by  $\theta$ , and the loss is computed over  $N$  training samples.

### 3.2.2 Pre-training via Data-Driven Losses and PDE Constraints

In this approach, we incorporate both data-driven losses and physics-based constraints (PDE residuals) during pre-training. The objective is to leverage available solution data while maintaining compliance with the underlying PDEs. The hybrid loss function is defined as:

$$\mathcal{L}_{\text{hybrid}}(\theta) = \alpha \mathcal{L}_{\text{data}}(\theta) + (1 - \alpha) \mathcal{L}_{\text{PDE}}(\theta), \quad (4)$$

where:

$$\mathcal{L}_{\text{data}}(\theta) = \frac{1}{M} \sum_{j=1}^M \|\mathcal{F}_\theta(f_j, \lambda_j) - u_j\|^2, \quad (5)$$

and  $u_j$  represents the ground-truth solution data. The weighting factor  $\alpha \in [0, 1]$  balances the contribution of the data and physics terms. This is similar to PINNs [20] but uses spectral derivatives instead of automatic differentiation, as the network does not explicitly take spatial discretization points as inputs.

### 3.3 Fine-tuning Strategy

After the pre-training phase, the model is fine-tuned using only data loss to adapt to specific tasks and improve accuracy for target PDE instances. Fine-tuning refines learned representations and optimizes performance for downstream tasks, including PDEs with shifted parameter distributions and unseen PDEs.

Given a dataset  $\mathcal{D}_{\text{fine}} = \{(f_j, u_j^0, \lambda_j, u_j)\}_{j=1}^M$ , where  $f_j$  represents the forcing function,  $u_j^0$  is the initial condition (in the case of time-dependent problems),  $\lambda_j$  denotes the PDE parameters, and  $u_j$  is the corresponding ground-truth solution, the fine-tuning process minimizes the following data-driven loss:

$$\mathcal{L}_{\text{data}}(\theta) = \frac{1}{M} \sum_{j=1}^M \|\mathcal{F}_\theta(f_j, u_j^0, \lambda_j) - u_j\|^2, \quad (6)$$

where  $\mathcal{F}_\theta$  represents the neural network parameterized by  $\theta$ . Fine-tuning with data loss allows the model to adapt efficiently to specific PDE instances, leveraging the representations learned during pre-training while focusing on task-specific accuracy.

## 4 Experimental Setup

In this section, we present the experimental setup for our evaluations. We introduce dataset augmentation for both pre-training and downstream tasks, the baseline models used for comparison, and the evaluation metrics applied to assess the performance of the models. Datasets creation procedure, and comprehensive implementation details, encompassing the training and inference procedures and the computational configurations, are provided in Appendix B.

### 4.1 Data Augmentation

We incorporate input normalization, as proposed in [22], since it has been shown to enhance the generalization capabilities of FNO models, particularly in scenarios where input channels exhibit different scales.

To assess the robustness of the model against noise during fine-tuning, we introduce noise into the solution space of the fine-tuning dataset to simulate real-world measurement inaccuracies. Specifically, we add additive white Gaussian noise to the solution, formulated as

$$u_{\text{noisy}} = u + \sigma \cdot \text{std}(u) \cdot \epsilon, \quad (7)$$

Table 1: Coefficient ranges for each dataset used in the pre-training and downstream tasks. Diffusion Coefficient  $\mathbf{D}$ , Advection-Diffusion Ratio  $\Psi$ , Wave-number  $\omega$ , Reaction Coefficient  $r$ , Velocity Vector  $\mathbf{v}$ . The coefficient ranges are given as (min, max), while coefficients without corresponding solutions in a dataset are given as  $\emptyset$ -subscript and called synthetic.

Training-Stage	Dataset	Poisson	Advection-Diffusion	Helmholtz	Reaction-Diffusion	Reaction-Advection-Diffusion
Pre-Training	Expensive	$\mathbf{D} \sim (1, 5)$	$\Psi \sim (0.2, 1)$	$\omega \sim (1, 10)$		
	Synthetic	$\mathbf{D}_\emptyset \sim (1, 5)$	$\Psi_\emptyset \sim (0.2, 1)$	$\omega_\emptyset \sim (1, 10)$		
	Extended	$\mathbf{D} \sim (1, 5)$ $\mathbf{D}_\emptyset \sim (15, 20)$	$\Psi \sim (0.2, 1)$ $\Psi_\emptyset \sim (4, 5)$	$\omega \sim (1, 15)$		
Downstream	ID	$\mathbf{D} \sim (1, 2.5)$	$\Psi \sim (0.2, 0.4)$	$\omega \sim (1, 5)$		
	Slight-OOD	$\mathbf{D} \sim (2.5, 7.5)$	$\Psi \sim (0.4, 1.6)$	$\omega \sim (2, 12)$	$\mathbf{D} \sim (5, 10), r \sim (-1, 1)$	$\mathbf{D} \sim (5, 10), \mathbf{v} \sim (0.1, 1), r \sim (-1, 1)$
	Medium-OOD	$\mathbf{D} \sim (7.5, 12.5)$	$\Psi \sim (2, 3)$	$\omega \sim (10, 13)$		
	High-OOD	$\mathbf{D} \sim (15, 20)$	$\Psi \sim (4, 5)$	$\omega \sim (12, 15)$		

where  $\epsilon \sim \mathcal{N}(0, 1)$  represents a standard normal random variable, and  $\sigma$  denotes the noise level. We conduct experiments using different noise levels:  $\sigma = 0.01$ , simulating high-precision measurements,  $\sigma = 0.05$  and  $\sigma = 0.1$  to reflect typical measurement uncertainties, and  $\sigma = 0.2$  to represent highly noisy conditions. This approach comprehensively evaluates the model’s robustness to various noise levels within the solution space, providing insights into its resilience under realistic conditions.

## 4.2 Baselines, Pre-training Approaches, and Datasets

We compare our method against two baseline models and introduce two constraint-aware pre-training strategies. All models are based on the FNO architecture, utilize input normalization, and are fine-tuned on downstream tasks using the  $\mathcal{L}_{\text{data}}$  loss.

### Baselines.

- **Scratch (baseline):** Trained solely on each downstream task without any pre-training. This serves as our primary baseline to assess the impact of pre-training.
- **Data-Loss (baseline):** Pre-trained using only the data-driven loss  $\mathcal{L}_{\text{data}}$ , following the approach in [22], without incorporating physics-based constraints. It is subsequently fine-tuned on each downstream task.

### Pre-training Approaches.

- **Physics-Loss (ours):** Pre-trained exclusively using PDE residuals, without any access to solution data. This enables leveraging physics knowledge in the absence of labeled data.
- **Hybrid-Loss (ours):** Pre-trained using both data loss and PDE residuals. For PDEs where solution data is available, both losses are used; otherwise, the model relies solely on PDE residuals. This flexible strategy enables broader pre-training across diverse PDEs without requiring complete solution data.

**Pre-training Datasets.** We use the following datasets for pre-training, which include data for the Poisson, Advection-Diffusion, and Helmholtz equations only. The remaining PDEs listed in Table 1 are reserved exclusively for evaluation.

- **Expensive:** Contains full solution data for selected PDEs, with coefficients sampled from the pre-training range described in Table 1. This dataset is used for both training and evaluation baselines.
- **Synthetic:** Contains only PDE residuals with no solution data. It is generated by sampling coefficients and source terms from the pre-training range described in Table 1. This dataset is used in the Physics-Loss pre-training.
- **Extended:** Combines the expensive and synthetic datasets, but extends the synthetic portion by sampling coefficients from both ID and out-of-distribution (OOD) ranges. This enables the model to experience a broader range of physical conditions during pre-training.

### 4.3 Evaluation Metrics

To evaluate the performance of the models, we employ three distinct metrics: the  $\mu_{\ell_2}$  error, the  $L_{\infty}$  error, and the fRMSE. The  $\mu_{\ell_2}$  error quantifies the mean relative error between the predicted and ground truth solutions, defined as

$$\mu_{\ell_2} = \frac{1}{N} \sum_{i=1}^N \frac{\|u_i - \hat{u}_i\|_2}{\|u_i\|_2}, \quad (8)$$

which captures the average deviation from the ground truth. The  $L_{\infty}$  error measures the maximum error between the predicted and ground truth solutions, defined as

$$L_{\infty} = \max_i |u_i - \hat{u}_i|, \quad (9)$$

which reflects the maximum deviation from the ground truth. The fRMSE describes the root mean square error in the frequency domain, defined as

$$\text{fRMSE} = \frac{1}{N} \sum_{i=1}^N \frac{\sqrt{\sum_{k_{\min}}^{k_{\max}} |\mathcal{F}(\hat{u}_i) - \mathcal{F}(u_i)|^2}}{k_{\max} - k_{\min} + 1}, \quad (10)$$

where  $\mathcal{F}$  denotes the Fourier transform, and  $k_{\max}$  and  $k_{\min}$  are the maximum and minimum indices of the Fourier transform, respectively, with  $N$  representing the number of samples. We adopt a partitioning approach similar to that in [24] for the classification of low, middle, and high-frequency regions. This classification allows us to quantify the model’s ability to capture global, large-scale features, medium-scale features, and periodicity, as well as small-scale features and noise corresponding to the low, middle, and high-frequency regions, respectively.

## 5 Empirical Results

In this section, we systematically evaluate the generalization and robustness of the proposed approaches across different learning scenarios. We evaluate the model’s performance using the metrics introduced in Sec. 4.3 across the scenarios described below.

In Section 5.1, we begin with an analysis of the zero-shot generalization capabilities of the pre-trained model on both in-distribution (ID) and out-of-distribution (OOD) downstream tasks. We further examine how the model performs as tasks become progressively OOD by shifting PDE parameters and operator characteristics.

In Section 5.2, we investigate n-shot learning, where the pre-trained model is fine-tuned on limited data for both ID and OOD tasks. This section also evaluates the robustness of the model by introducing noise into the solution space of Advection-Diffusion and Helmholtz tasks. This analysis helps determine whether constraint-aware pre-training enhances the model’s stability in real-world scenarios where measurement errors and data imperfections are common.

In Section 5.3, we evaluate the model’s generalization to PDEs that were not seen during pre-training, i.e., the Darcy equation, the Reaction-Diffusion, and Reaction-Advection-Diffusion systems. These tasks introduce significant deviations from the pre-training distribution due to changes in coefficients, problem formulations, and boundary conditions, allowing us to assess the model’s ability to extrapolate to previously unseen PDEs.

This structured evaluation provides a comprehensive understanding of how well the proposed approach generalizes to new physics, adapts to unseen PDEs, and maintains robustness under noisy conditions.

### 5.1 Exploring Zero-Shot Generalization

**Assessing Zero-Shot Performance Across Downstream Tasks.** We conduct an initial evaluation to determine whether the constraint-aware approaches improve zero-shot generalization. Specifically, we examine the performance of a pre-trained model on downstream tasks that are either ID or OOD relative to the pre-training data. We analyze the Poisson, Advection-Diffusion, and Helmholtz tasks, with ID and OOD ranges for each metric detailed in Table 1. Table 2 compares the performance of constraint-aware pre-training approaches and baseline models trained on the expensive dataset. In contrast, Table 3 evaluates the impact of extending the dataset with synthetic data and a broader coefficient range on the performance of the pre-trained models.

Table 2:  $\mu_{\ell_2}$  and  $L_{\infty}$  metrics for zero-shot on in-distribution (ID) and out-of-distribution (OOD) parametrization of downstream tasks corresponding to the same PDEs used during pre-training. The models are pre-trained on the expensive pre-training dataset, except for Physics-Loss, which is pre-trained on the synthetic data. Two best models are highlighted.

Metric	Model	Pre-Training	Poisson			Advection-Diffusion			Helmholtz					
			ID	Slight-OOD	Medium-OOD	High-OOD	ID	Slight-OOD	Medium-OOD	High-OOD	ID	Slight-OOD	Medium-OOD	High-OOD
$\mu_{\ell_2}$	Scratch	-	1.0080	1.1736	1.0061	1.8586	1.0005	1.1850	1.2476	<b>1.3294</b>	1.0137	1.1039	1.5014	1.3249
	Data-Loss	0.0092	0.0025	0.0102	<b>0.1225</b>	<b>0.5750</b>	0.0068	0.0434	<b>0.8813</b>	<b>1.8948</b>	0.0040	<b>0.2448</b>	<b>1.2165</b>	<b>1.2121</b>
	Physics-Loss	<b>0.0080</b>	<b>0.0005</b>	<b>0.0055</b>	0.1584	1.2473	<b>0.0020</b>	<b>0.0174</b>	2.3344	22.068	<b>0.0017</b>	0.3610	2.0163	4.3618
	Hybrid-Loss	<b>0.0019</b>	<b>0.0005</b>	<b>0.0067</b>	<b>0.1326</b>	<b>0.7091</b>	<b>0.0025</b>	<b>0.0260</b>	<b>1.2705</b>	4.1350	<b>0.0007</b>	<b>0.2363</b>	<b>1.2177</b>	<b>1.1825</b>
$L_{\infty}$	Scratch	-	0.8171	0.4959	0.4243	<b>0.4702</b>	0.6644	0.6286	<b>0.9239</b>	<b>1.6784</b>	7.8970	7.5244	<b>1.5851</b>	<b>0.6475</b>
	Data-Loss	0.0666	0.0035	0.0182	0.1661	<b>0.7197</b>	0.0060	<b>0.1172</b>	<b>1.0009</b>	<b>2.0415</b>	0.0557	<b>1.5207</b>	<b>1.6423</b>	0.6822
	Physics-Loss	<b>0.0485</b>	<b>0.0007</b>	<b>0.0101</b>	<b>0.1493</b>	0.7453	<b>0.0021</b>	<b>0.0580</b>	6.3186	20.638	<b>0.0211</b>	1.6237	1.7669	2.0586
	Hybrid-Loss	<b>0.0028</b>	<b>0.0007</b>	<b>0.0124</b>	<b>0.0836</b>	<b>0.3155</b>	0.0023	0.1325	1.6630	2.7702	<b>0.0036</b>	<b>1.5212</b>	1.6534	<b>0.6385</b>

Table 3: Zero-shot performance on in-distribution (ID) and out-of-distribution (OOD) parameterizations for downstream tasks involving the same PDEs used during pre-training. We report the mean  $\ell_2$  error ( $\mu_{\ell_2}$ ) and maximum error ( $L_{\infty}$ ), comparing constraint-aware pre-training using the expensive and extended datasets. Two best models are highlighted.

Metric	Model	Pre-Training	Poisson			Advection-Diffusion			Helmholtz					
			ID	Slight-OOD	Medium-OOD	High-OOD	ID	Slight-OOD	Medium-OOD	High-OOD	ID	Slight-OOD	Medium-OOD	High-OOD
$\mu_{\ell_2}$	Physics-Loss (synthetic)	0.0080	<b>0.0005</b>	0.0055	0.1584	1.2473	<b>0.0020</b>	<b>0.0174</b>	2.3344	22.068	<b>0.0017</b>	0.3610	2.0163	4.3618
	Physics-Loss (extended)	0.0051	0.0012	<b>0.0052</b>	<b>0.1222</b>	<b>0.0033</b>	0.0065	0.0376	<b>0.0847</b>	<b>0.0302</b>	0.0027	<b>0.0059</b>	<b>0.0125</b>	<b>0.0238</b>
	Hybrid-Loss (expensive)	<b>0.0019</b>	<b>0.0005</b>	0.0067	0.1326	<b>0.7091</b>	<b>0.0025</b>	<b>0.0260</b>	1.2705	4.1350	<b>0.0007</b>	0.2363	1.2177	1.1825
	Hybrid-Loss (extended)	<b>0.0047</b>	0.0008	<b>0.0030</b>	<b>0.0089</b>	<b>0.0034</b>	0.0049	0.0276	<b>0.0741</b>	<b>0.0309</b>	0.0033	<b>0.0063</b>	<b>0.0082</b>	<b>0.0146</b>
$L_{\infty}$	Physics-Loss (synthetic)	0.0485	<b>0.0007</b>	0.0101	0.1493	0.7453	<b>0.0021</b>	<b>0.0580</b>	6.3186	20.638	<b>0.0211</b>	1.6237	1.7669	2.0586
	Physics-Loss (extended)	<b>0.0136</b>	0.0017	<b>0.0063</b>	<b>0.0079</b>	<b>0.0019</b>	0.0071	0.0725	<b>0.1543</b>	<b>0.1325</b>	0.0280	<b>0.0314</b>	<b>0.0302</b>	<b>0.0305</b>
	Hybrid-Loss (expensive)	<b>0.0028</b>	<b>0.0007</b>	0.0124	0.0836	0.3155	<b>0.0023</b>	0.1325	1.6630	2.7702	<b>0.0036</b>	1.5212	1.6534	0.6385
	Hybrid-Loss (extended)	0.0141	0.0010	<b>0.0030</b>	<b>0.0050</b>	<b>0.0023</b>	0.0044	<b>0.0419</b>	0.1120	<b>0.1218</b>	0.0406	<b>0.0360</b>	0.0270	<b>0.0185</b>

Although all pre-training approaches enhance zero-shot generalization compared to the Scratch model, constraint-aware pre-training significantly improves performance in both ID and OOD tasks. This suggests that incorporating PDE residuals helps the model better capture the underlying solution space structure. In the Helmholtz task, slight variations in the wave number drastically alter the solution space, creating a more challenging OOD scenario. The Physics-Loss approach struggles in these cases, indicating its sensitivity to significant deviations from the pre-training distribution. However, the data-driven component in the Hybrid-Loss approach helps mitigate this effect. Moreover, the Hybrid-Loss approach demonstrates a significant improvement over other constraint-aware and baseline models across all OOD settings, while experiencing only minimal decrease in performance in the ID settings. This suggests that the inclusion of data points without corresponding solutions during the pre-training stages enables the model to learn a significant better representation of the underlying systems through the use of PDE residuals, thereby enhancing its generalization capabilities.

**Zero-Shot Performance in OOD Regions.** We evaluate zero-shot performance by testing the pre-trained model on progressively OOD datasets. The results for High-OOD are included in Table 2 and Table 3. The Physics-Loss model shows a sharp decline in performance, particularly in Advection-Diffusion and Helmholtz tasks, where even slight OOD shifts cause failures. The Hybrid-Loss model follows a similar trend but performs better in High-OOD scenarios, while the Data-Loss model is more robust to coefficient variations. These results indicate that Physics-Loss is highly sensitive to distribution shifts, and incorporating data loss in Hybrid-Loss helps improve generalization. The Hybrid-Loss model effectively mitigates this issue by learning from a broader range of coefficients through the application of PDE residuals in the pre-training step (extended dataset), compared to models which rely on data loss. This significantly enhances its generalization capabilities, even beyond its trained distribution. For further details, see Appendix C.1.

## 5.2 n-Shot Generalization to New Physics

Here, we assess the n-shot performance of the pre-trained model on Advection-Diffusion and Helmholtz tasks, covering both ID and OOD ranges (Table 1). Additionally, we evaluate model robustness by testing on noisy solution spaces for these tasks.

**n-Shot Learning Across Various Degrees of Out-of-Distribution.** We conduct experiments to evaluate the n-shot generalization of our pre-trained models, fine-tuning them across varying levels of OOD,

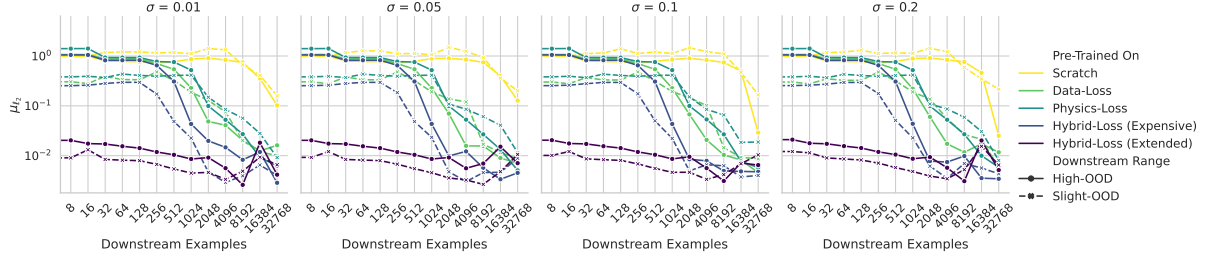


Figure 2: Evaluation of the  $\mu_{\ell_2}$  metric for varying degrees of noise in the solution domain for the OOD pushed datasets in the Helmholtz task. From left to right,  $\sigma$  takes the form of 0.01, 0.05, 0.1, and 0.2. The Data-Loss model is pre-trained on the expensive dataset, whereas the Physics-Loss model is pre-trained on the synthetic dataset. For the Hybrid-Loss model, we incorporate both pre-training strategies.

as shown in Table 1. The results presented in Tables 4 illustrate the performance of pre-trained models on the expensive and extended datasets for the Helmholtz and Advection-Diffusion tasks, following fine-tuning with  $2^{15}$  downstream examples. These findings indicate that constraint-aware models consistently surpass both baselines across almost all out-of-distribution (OOD) levels. Our investigations reveal that these models are more effective at learning the dominant frequencies in the solution space, enabling them to generalize better to new problem settings, including those with significant OOD variations. Additionally, extending the coefficient ranges of pre-training PDEs enhances performance on downstream tasks, particularly in high-OOD settings. This improvement stems from better representation learning enabled by diversifying the pre-training data with cheap synthetic samples. For a detailed analysis, please refer to Appendix C.2.

Table 4:  $\mu_{\ell_2}$  and  $L_{\infty}$  results of models using  $2^{15}$  downstream examples for fine-tuning on the Advection-Diffusion and Helmholtz task with ID and OOD parametrization. We evaluate the effect of pre-training approaches and datasets on the downstream tasks performance.

Metric	Model	Advection-Diffusion				Helmholtz			
		ID	Slight-OOD	Medium-OOD	High-OOD	ID	Slight-OOD	Medium-OOD	High-OOD
$\mu_{\ell_2}$	Scratch	0.0022	0.0321	0.2221	0.2537	0.0058	0.2367	0.0425	0.0187
	Data-Loss(Expensive)	0.0025	0.0121	0.0689	0.1385	0.0012	0.0079	<b>0.0057</b>	0.0058
	Physics-Loss(Synthetic)	<b>0.0011</b>	<b>0.0065</b>	0.0259	0.1288	0.0005	0.0108	0.0074	0.0083
	Hybrid-Loss(Expensive)	<b>0.0013</b>	0.0077	0.0427	0.1598	0.0005	<b>0.0030</b>	0.0060	<b>0.0029</b>
	Physics-Loss(Extended)	0.0014	<b>0.0066</b>	<b>0.0256</b>	<b>0.1118</b>	<b>0.0005</b>	<b>0.0038</b>	<b>0.0031</b>	<b>0.0049</b>
	Hybrid-Loss(Extended)	0.0016	0.0070	<b>0.0221</b>	<b>0.0956</b>	<b>0.0005</b>	0.0082	0.0059	0.0119
$L_{\infty}$	Scratch	0.0024	0.0645	0.4706	1.0246	0.1356	0.9069	0.1253	0.1070
	Data-Loss(Expensive)	0.0024	0.0159	0.2007	0.8178	0.0107	0.0227	0.0112	0.0108
	Physics-Loss(Synthetic)	<b>0.0010</b>	<b>0.0053</b>	0.0832	0.7704	0.0022	0.0295	0.0109	0.0096
	Hybrid-Loss(Expensive)	<b>0.0013</b>	0.0091	0.2087	0.8891	0.0023	<b>0.0061</b>	<b>0.0079</b>	<b>0.0030</b>
	Physics-Loss(Extended)	0.0014	<b>0.0055</b>	<b>0.0239</b>	<b>0.6164</b>	<b>0.0015</b>	<b>0.0069</b>	<b>0.0038</b>	<b>0.0045</b>
	Hybrid-Loss(Extended)	0.0016	0.0057	0.0403	<b>0.5908</b>	<b>0.0016</b>	0.0169	0.0089	0.0150

**n-Shot with Noisy Solution Space.** We examine the impact of noisy data during fine-tuning across various PDE systems. Constraint-aware models consistently outperform the baselines at all noise levels and for all PDEs. Even under substantial noise, the constraint-aware models maintain performance comparable to their noise-free counterparts. Notably, in some cases—such as the Helmholtz task in a high-OOD setting with  $2^{15}$  samples—the Physics-Loss model surpasses the Data-Loss model despite significant noise in the solution space. See Figure 2 for Helmholtz results.

These findings indicate that constraint-aware training, which combines PDE and data loss, enhances the robustness of the models. A comparison of the fRMSE metric (c.f. Figure 27 and Figure 28 in Appendix C.3) for slight and high OOD settings in the Helmholtz equation with noisy solution spaces shows that constraint-aware models consistently achieve lower error rates at higher frequencies. Since additive white Gaussian noise is inherently a high-frequency signal, this suggests that these models effectively capture small-scale solution components, explaining their superior performance over the models pre-training solely on data-driven losses. Similar trends are observed for the Advection-Diffusion equation, with corresponding results provided in Appendix C.3.

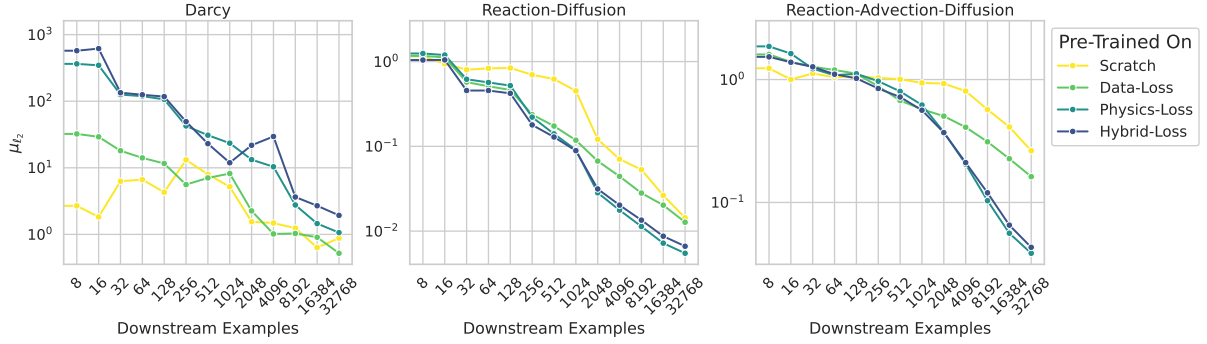


Figure 3: The  $\mu_{\ell_2}$  metrics for the downstream tasks of Darcy, Reaction-Diffusion, and Reaction-Advection-Diffusion, respectively, with an increasing number of downstream examples used during fine-tuning. While the Physics-Loss and Hybrid-Loss models are pre-trained on the extended pre-training dataset, the Data-Loss model is pre-trained on the expensive dataset.

### 5.3 Shifting Focus to Unseen PDEs

We evaluate the performance of the pre-trained models on PDEs unseen during pre-training, namely the Reaction-Diffusion, Reaction-Advection-Diffusion, and Darcy equations. These PDEs exhibit significant deviations from the pre-training distribution. These systems differ in problem formulation, transitioning from steady-state PDEs to Initial Value Problems, and introducing new coefficient structures. Additionally, while all other PDEs in our study assume periodic boundary conditions, the Darcy equation employs Dirichlet boundary conditions, requiring the pre-trained models to adapt their input channels and internal representations to accommodate these fundamental changes in boundary conditions and coefficient distributions. The results are illustrated in Figure 3. In the Reaction-Diffusion task, constraint-aware models outperform the baselines, achieving performance levels comparable to previous tasks (c.f. Figure 10, Figure 13, Figure 16 and Figure 19). In the Reaction-Advection-Diffusion task, the Hybrid-Loss approach outperforms other models, especially in scenarios with larger data regimes. This result underscores the advantage of pre-training on a broader range of PDEs and diverse data, even in the absence of solution data, in enhancing model transferability across domains. However, in the Darcy task, all models struggle, with constraint-aware models performing the worst, indicating challenges in adapting to non-periodic boundary conditions. The strong generalization of the constraint-aware models in the Reaction-Diffusion task can be attributed to the structural similarity between its PDE formulation and the pre-training data from the Poisson and Advection-Diffusion tasks. In contrast, fRMSE results for the Reaction-Advection-Diffusion and Darcy tasks (see Figure 31 or Figure 32 in Appendix C.4) show that the Physics-Loss model struggles to reduce errors in the dominant frequency ranges, suggesting that the constraint-aware training may not effectively transfer to these tasks if the data provided in the pre-training stages is insufficiently diverse. This highlights the use of a hybrid approach through the use of PDE residuals on synthetic data to increase the diversity of datasets. Our results indicate that the Physics-Loss term may lead to overfitting to the frequency distributions present in the pre-training data, which differ significantly from those in the Reaction-Advection-Diffusion and Darcy equations. In contrast, the Hybrid-Loss model, which incorporates a data-driven component, and higher diversity in samples for the hybrid approach specifically, exhibits better generalization and achieves lower error rates in systems with substantial structural differences. This trend aligns with the results observed in OOD Helmholtz tasks (see Figure 16 and Figure 19), where the hybrid loss model showed superior adaptability. Finally, the poor performance across all models on the Darcy equation can be attributed to its non-periodic boundary conditions, which are inherently incompatible with the FNO architecture. This highlights a fundamental limitation of this approach in handling certain boundary condition types.

## 6 Conclusion

This work takes a step toward SciFMs by proposing a data-efficient approach that compensates for missing solution data using PDE residuals, making the development of large SciFMs more feasible. Through extensive evaluations, we demonstrate that this method enables models to learn rich, transferable representations without solely relying on large PDE solution datasets. Our results show that pre-training

with PDE constraints enhances generalization in four key areas: i) Adapting to new physics (i.e., PDEs seen in training but with shifted parameters), ii) Generalizing to entirely new PDE operators, iii) Transferring from simpler to more complex problems, and iv) Maintaining robustness under noisy fine-tuning data. Compared to non-constraint-aware baselines, our approach consistently improves performance across these benchmarks. However, challenges remain in generalizing across boundary conditions, particularly non-periodic BCs, where models struggle—most notably in the Darcy equation. Whether this limitation arises from architectural constraints (e.g., FNO) or reflects a fundamental challenge in PDE transfer learning remains an open question. Having validated constraint-aware pre-training, the next step is to scale this approach to larger models, leveraging these insights to develop data-efficient, broadly generalizable SciFMs capable of solving a wide range of PDE-driven problems.

## Acknowledgements

This work is funded by Deutsche Forschungsgemeinschaft (DFG, German Research Foundation) under Germany’s Excellence Strategy - EXC 2075 – 390740016. We acknowledge the support by the Stuttgart Center for Simulation Science (SimTech). Additionally, the authors gratefully acknowledge the computing time provided on the high-performance computer HoreKa by the National High-Performance Computing Center at KIT (NHR@KIT). This center is jointly supported by the Federal Ministry of Education and Research and the Ministry of Science, Research and the Arts of Baden-Württemberg, as part of the National High-Performance Computing (NHR) joint funding program (<https://www.nhr-verein.de/en/our-partners>). HoreKa is partly funded by the German Research Foundation (DFG).

## References

- [1] Josh Achiam, Steven Adler, Sandhini Agarwal, Lama Ahmad, Ilge Akkaya, Florencia Leoni Aleman, Diogo Almeida, Janko Altenschmidt, Sam Altman, Shyamal Anadkat, et al. Gpt-4 technical report. *arXiv preprint arXiv:2303.08774*, 2023.
- [2] Tom Brown, Benjamin Mann, Nick Ryder, Melanie Subbiah, Jared D Kaplan, Prafulla Dhariwal, Arvind Neelakantan, Pranav Shyam, Girish Sastry, Amanda Askell, et al. Language models are few-shot learners. *Advances in neural information processing systems*, 33:1877–1901, 2020.
- [3] Wuyang Chen, Jialin Song, Pu Ren, Shashank Subramanian, Dmitriy Morozov, and Michael W Mahoney. Data-efficient operator learning via unsupervised pretraining and in-context learning. *arXiv preprint arXiv:2402.15734*, 2024.
- [4] Alexey Dosovitskiy, Lucas Beyer, Alexander Kolesnikov, Dirk Weissenborn, Xiaohua Zhai, Thomas Unterthiner, Mostafa Dehghani, Matthias Minderer, Georg Heigold, Sylvain Gelly, Jakob Uszkoreit, and Neil Houlsby. An image is worth 16x16 words: Transformers for image recognition at scale. In *International Conference on Learning Representations*, 2021.
- [5] Sergei K Godunov and I Bohachevsky. Finite difference method for numerical computation of discontinuous solutions of the equations of fluid dynamics. *Matematicheskij sbornik*, 47(3):271–306, 1959.
- [6] Somdatta Goswami, Minglang Yin, Yue Yu, and George Em Karniadakis. A physics-informed variational deeponet for predicting crack path in quasi-brittle materials. *Computer Methods in Applied Mechanics and Engineering*, 391:114587, 2022.
- [7] Maximilian Herde, Bogdan Raonić, Tobias Rohner, Roger Käppeli, Roberto Molinaro, Emmanuel de Bézenac, and Siddhartha Mishra. Poseidon: Efficient foundation models for pdes. *arXiv preprint arXiv:2405.19101*, 2024.
- [8] Joel Ho, Nick Pepper, and Tim Dodwell. Probabilistic machine learning to improve generalisation of data-driven turbulence modelling. *Computers & Fluids*, 284:106443, 2024.
- [9] George Em Karniadakis, Ioannis G Kevrekidis, Lu Lu, Paris Perdikaris, Sifan Wang, and Liu Yang. Physics-informed machine learning. *Nature Reviews Physics*, 3(6):422–440, 2021.
- [10] Nikola Kovachki, Zongyi Li, Burigede Liu, Kamyar Azizzadenesheli, Kaushik Bhattacharya, Andrew Stuart, and Anima Anandkumar. Neural operator: Learning maps between function spaces with applications to pdes. *Journal of Machine Learning Research*, 24(89):1–97, 2023.
- [11] Aditi Krishnapriyan, Amir Gholami, Shandian Zhe, Robert Kirby, and Michael W Mahoney. Characterizing possible failure modes in physics-informed neural networks. *Advances in neural information processing systems*, 34:26548–26560, 2021.
- [12] Zongyi Li, Nikola Kovachki, Kamyar Azizzadenesheli, Burigede Liu, Kaushik Bhattacharya, Andrew Stuart, and Anima Anandkumar. Fourier neural operator for parametric partial differential equations. *arXiv preprint arXiv:2010.08895*, 2020.
- [13] Zongyi Li, Hongkai Zheng, Nikola Kovachki, David Jin, Haoxuan Chen, Burigede Liu, Kamyar Azizzadenesheli, and Anima Anandkumar. Physics-informed neural operator for learning partial differential equations. *ACM/JMS Journal of Data Science*, 1(3):1–27, 2024.
- [14] Lu Lu, Pengzhan Jin, Guofei Pang, Zhongqiang Zhang, and George Em Karniadakis. Learning nonlinear operators via deeponet based on the universal approximation theorem of operators. *Nature machine intelligence*, 3(3):218–229, 2021.
- [15] Michael McCabe, Bruno Régaldo-Saint Blanchard, Liam Holden Parker, Ruben Ohana, Miles Cranmer, Alberto Bietti, Michael Eickenberg, Siavash Golkar, Geraud Krawezik, Francois Lanusse, et al. Multiple physics pretraining for physical surrogate models. *arXiv preprint arXiv:2310.02994*, 2023.
- [16] Apostolos F Psaros, Xuhui Meng, Zongren Zou, Ling Guo, and George Em Karniadakis. Uncertainty quantification in scientific machine learning: Methods, metrics, and comparisons. *Journal of Computational Physics*, 477:111902, 2023.

[17] Alec Radford, Jong Wook Kim, Chris Hallacy, Aditya Ramesh, Gabriel Goh, Sandhini Agarwal, Girish Sastry, Amanda Askell, Pamela Mishkin, Jack Clark, et al. Learning transferable visual models from natural language supervision. In *International conference on machine learning*, pages 8748–8763. PMLR, 2021.

[18] Alec Radford, Jeffrey Wu, Rewon Child, David Luan, Dario Amodei, Ilya Sutskever, et al. Language models are unsupervised multitask learners. *OpenAI blog*, 1(8):9, 2019.

[19] Md Ashiqur Rahman, Robert Joseph George, Mogab Elleithy, Daniel Leibovici, Zongyi Li, Boris Bonev, Colin White, Julius Berner, Raymond A Yeh, Jean Kossaifi, et al. Pretraining codomain attention neural operators for solving multiphysics pdes. *arXiv preprint arXiv:2403.12553*, 2024.

[20] Maziar Raissi, Paris Perdikaris, and George E Karniadakis. Physics-informed neural networks: A deep learning framework for solving forward and inverse problems involving nonlinear partial differential equations. *Journal of Computational physics*, 378:686–707, 2019.

[21] Dong H Song and Daniel M Tartakovsky. Transfer learning on multifidelity data. *Journal of Machine Learning for Modeling and Computing*, 3(1), 2022.

[22] Shashank Subramanian, Peter Harrington, Kurt Keutzer, Wahid Bhimji, Dmitriy Morozov, Michael W Mahoney, and Amir Gholami. Towards foundation models for scientific machine learning: Characterizing scaling and transfer behavior. In A. Oh, T. Naumann, A. Globerson, K. Saenko, M. Hardt, and S. Levine, editors, *Advances in Neural Information Processing Systems*, volume 36, pages 71242–71262. Curran Associates, Inc., 2023.

[23] Makoto Takamoto, Timothy Praditia, Raphael Leiteritz, Dan MacKinlay, Francesco Alesiani, Dirk Pflüger, and Mathias Niepert. PDEBench Datasets, 2022.

[24] Makoto Takamoto, Timothy Praditia, Raphael Leiteritz, Daniel MacKinlay, Francesco Alesiani, Dirk Pflüger, and Mathias Niepert. Pdebench: An extensive benchmark for scientific machine learning. In S. Koyejo, S. Mohamed, A. Agarwal, D. Belgrave, K. Cho, and A. Oh, editors, *Advances in Neural Information Processing Systems*, volume 35, pages 1596–1611. Curran Associates, Inc., 2022.

[25] Hengjie Wang, Robert Planas, Aparna Chandramowlishwaran, and Ramin Bostanabad. Mosaic flows: A transferable deep learning framework for solving pdes on unseen domains. *Computer Methods in Applied Mechanics and Engineering*, 389:114424, 2022.

[26] Sifan Wang, Shyam Sankaran, and Paris Perdikaris. Respecting causality for training physics-informed neural networks. *Computer Methods in Applied Mechanics and Engineering*, 421:116813, 2024.

[27] Chenxi Wu, Min Zhu, Qinyang Tan, Yadhu Kartha, and Lu Lu. A comprehensive study of non-adaptive and residual-based adaptive sampling for physics-informed neural networks. *Computer Methods in Applied Mechanics and Engineering*, 403:115671, 2023.

[28] Chen Xu, Ba Trung Cao, Yong Yuan, and Günther Meschke. Transfer learning based physics-informed neural networks for solving inverse problems in engineering structures under different loading scenarios. *Computer Methods in Applied Mechanics and Engineering*, 405:115852, 2023.

[29] Wuzhe Xu, Yulong Lu, and Li Wang. Transfer learning enhanced deeponet for long-time prediction of evolution equations. In *Proceedings of the AAAI Conference on Artificial Intelligence*, volume 37, pages 10629–10636, 2023.

[30] Liu Yang, Siting Liu, Tingwei Meng, and Stanley J Osher. In-context operator learning with data prompts for differential equation problems. *Proceedings of the National Academy of Sciences*, 120(39):e2310142120, 2023.

[31] Olgierd Cecil Zienkiewicz, Robert Leroy Taylor, Perumal Nithiarasu, and JZ Zhu. *The finite element method*, volume 3. Elsevier, 1977.

## A Training and Evaluation PDE Systems Setup

We examine six elliptical fundamental systems of partial differential equations (PDEs) that serve as essential components for various scientific and engineering applications. For pre-training, we use three steady-state PDEs: the Poisson, Advection-Diffusion, and Helmholtz equations. To evaluate our approach, we expand this set to include three time-dependent initial value problems: the Reaction-Diffusion, Advection-Reaction-Diffusion, and Darcy equations. Each system is defined over the spatial domain  $\Omega = [0, 1]^2$ , while the time-dependent problems evolve over the interval  $\tau = [0, 1]$ . Except for the Darcy equation, which employs Dirichlet boundary conditions, all other PDEs assume periodic boundary conditions. The source term is represented as  $f(\mathbf{x}, t)$ . The steady-state problems are designed to map the force function and PDE parameters to the corresponding steady-state solution. In contrast, the time-dependent problems aim to map the PDE parameters and initial conditions to the solution at  $t = 1$ , as outlined in this study:

**Poisson Equation:** We consider a classical elliptic PDE that models diffusion processes with a source term:

$$-\nabla \cdot \mathbf{D} \nabla u = f \quad \text{in } \Omega, \quad (11)$$

where  $u(\mathbf{x})$  is the unknown solution, and  $\mathbf{D}$  is the diffusion coefficient tensor that characterizes the material properties.

**Advection-Diffusion Equation:** This equation describes the steady-state interplay between advective and diffusive transport processes:

$$-\nabla \cdot \mathbf{D} \nabla u + \mathbf{v} \cdot \nabla u = f \quad \text{in } \Omega, \quad (12)$$

where  $\mathbf{v}$  is the velocity field capturing advection effects, and  $\mathbf{D}$  is the diffusion coefficient tensor. To assess the balance between advection and diffusion, a dimensionless number is defined [22]:

$$\Psi = \frac{\|\mathbf{v} \cdot \nabla u\|}{\|\nabla \cdot \mathbf{D} \nabla u\|}. \quad (13)$$

**Helmholtz Equation:** The Helmholtz equation models wave propagation and oscillatory phenomena commonly encountered in acoustics and electromagnetics:

$$-\Delta u + \omega u = f \quad \text{in } \Omega, \quad (14)$$

where  $\omega > 0$  is the wavenumber that controls the frequency of oscillations in the solution.

**Reaction-Diffusion Equation:** A steady-state reaction-diffusion system, which describes the distribution of chemical or biological species under diffusion and reaction processes:

$$\frac{\partial u}{\partial t} - \nabla \cdot \mathbf{D} \nabla u + R(u) = f, \quad \text{in } \Omega \times \tau, \quad (15)$$

where  $\mathbf{D}$  is the diffusion coefficient tensor, and the reaction term  $R(u)$  models localized changes due to interactions such as chemical reactions or biological processes.

**Reaction-Advection-Diffusion Equation:** This PDE captures the combined effects of advection, diffusion, and reaction processes, which are commonly encountered in environmental and industrial applications:

$$\frac{\partial u}{\partial t} - \nabla \cdot \mathbf{D} \nabla u + \mathbf{v} \cdot \nabla u + R(u) = f \quad \text{in } \Omega \times \tau, \quad (16)$$

where  $\mathbf{v}$  is the velocity field capturing advection effects,  $\mathbf{D}$  is the diffusion coefficient tensor, and  $R(u)$  is the reaction term.

**Darcy Equation:** The Darcy equation describes fluid flow through porous media and is fundamental in hydrogeology and petroleum engineering:

$$\begin{aligned} \frac{\partial p}{\partial t} - \nabla \cdot (\mathbf{K} \nabla p) &= f \quad \text{in } \Omega \times \tau, \\ \mathcal{B}(p) &= 0 \quad \text{in } \mathbf{x} \in \partial\Omega \times \tau, \end{aligned} \quad (17)$$

where  $p(\mathbf{x})$  is the pressure field, and  $\mathbf{K}$  is the permeability tensor characterizing the medium's resistance to flow. For this problem setting, we consider the Dirichlet boundary condition.

## B Implementation Details

### B.1 Training and Inference Datasets Creation

**Source Function Sampling.** Source functions are generated using a linear combination of radial basis functions, expressed as  $f(x) = \sum_{i=1}^n \phi_i(x)p_i$ , where  $\phi_i(x)$  represents a Gaussian function centered at grid point  $x_i$ , and  $p_i$  is sampled from a uniform distribution,  $p_i \sim \mathcal{U}(0, 1)$ . Additionally, the source function is parameterized by the sparsity level  $s$ , which indicates the percentage of non-zero coefficients in the source function, effectively acting as a form of dropout. In our experiments, we maintain a fixed number of Gaussian functions  $n = 144$  and a set standard deviation  $\sigma = 1/32$ , while varying the sparsity level  $s$  from 20% to 80%. This approach enables the generation of a diverse set of source functions by adjusting the Gaussian basis functions' location, amplitude, and sparsity.

**Coefficient Sampling.** The diffusion coefficient tensor  $\mathbf{D}$  is constructed by sampling eigenvalues from a uniform distribution  $e \sim \mathcal{U}(e_{\min}, e_{\max})$ , leading to  $\mathbf{D} = R^T \text{diag}(e)R$ , where the rotation matrix  $R = \text{rot}(\theta)$  is generated using a random angle  $\theta \sim \mathcal{U}(0, 2\pi)$ . This allows control over the diffusion direction, while  $\text{diag}(e)$  governs anisotropy and diffusion extent. The velocity vector  $\mathbf{v}$  is sampled from  $\mathcal{U}(v_{\min}, v_{\max})$  for magnitude and adjusted by a random angle  $\theta \sim \mathcal{U}(0, 2\pi)$  for direction. The reaction coefficient  $r$  is sampled from  $\mathcal{U}(r_{\min}, r_{\max})$ , influencing reaction strength, and the wave number  $\omega$  is sampled from  $\mathcal{U}(\omega_{\min}, \omega_{\max})$ , affecting the solution's oscillatory behavior. For the Advection-Diffusion equation, the ratio  $\Psi$  is drawn from a uniform distribution  $\Psi \sim \mathcal{U}(\Psi_{\min}, \Psi_{\max})$ , regulating the balance between advection and diffusion. To attain the desired ratio, the velocity vector is scaled accordingly.

**Datasets Splitting.** For each dataset corresponding to a specific target PDE, we create a training set, a validation set, and a test set, comprising  $2^{15}$ ,  $2^{12}$ , and  $2^{12}$  samples, respectively, all at a resolution of  $128 \times 128$ . The source function is consistent across all datasets, while the coefficient tensor varies. See Table 1 for the ranges of coefficients used in each dataset for the experiments. For the Darcy equation, we use the dataset available at [23], as provided by PDEBench [24].

**Expensive, Synthetic and Extended Dataset.** Table 1 outlines three distinct datasets that vary in composition. All datasets maintain an equal total number of samples per operator, evenly distributed across the coefficient ranges. Datasets without a subscript include samples with solution data corresponding to the coefficient, force function, and operator, while datasets marked with the  $\emptyset$  subscript lack solution data. This distinction applies to the pre-training datasets labeled as expensive and synthetic, respectively. The extended dataset consists of both samples with and without solutions from their respective operators. As the number of samples per operator remains constant, this dataset contains only  $\frac{1}{3}$  of the samples with solutions compared to the expensive dataset. By incorporating this additional synthetic data, we simulate a scenario where generating the corresponding solutions is infeasible, while still allowing model to leverage these data points when possible.

**Downstream Dataset** . In contrast to the pre-training datasets, downstream tasks are treated as separate targets. During pre-training, a model simultaneously trains on the Poisson, Advection-Diffusion, and Helmholtz tasks. However, in the downstream task, only one operator is selected as the target for fine-tuning (e.g., Poisson ID with coefficient range  $\mathbf{D} \sim (1, 2.5)$ ). Since only the data loss  $\mathcal{L}_{\text{data}}$  is utilized for fine-tuning these models, all downstream datasets include samples with solution data. Additionally, to evaluate the model's performance at various n-shot points, we uniformly subsample the  $2^{15}$  samples from the corresponding downstream task dataset to obtain the desired number of examples for training. The validation and test sets are kept the same.

### B.2 Models

In our experimental setup, we implement four FNO models, including the proposed method, labeled as Physics-Loss and Hybrid-Loss, augmented with the physics loss term and an additional data loss term, respectively. We also include the baseline models from Section 4.2, Data-Loss and Scratch. The model embedding dimension and Fourier modes are fixed at 64 and 32, respectively. These values strike a favorable balance between performance and computational cost.

All inputs to the models are two-dimensional tensors, discretized on a grid of size  $h \times w = 128 \times 128$ , with the source function and coefficients serving as input channels  $c$ , forming an input tensor of shape

$\mathbb{R}^{h \times w \times c}$ . The models' output represents the PDE's solution space as a two-dimensional tensor of shape  $\mathbb{R}^{h \times w}$ . The pre-trained models have an input dimension of  $c = 8$ , corresponding to the number of source and coefficient channels required for all pre-training tasks. In contrast, the input channel dimension for the Scratch model is adjusted to reflect the minimum number of channels necessary for the downstream tasks.

### B.3 Training and Inference Procedure

For all training stages, we use the Adam optimizer with a cosine learning rate decay, training for a total of 500 epochs. The model with the lowest validation loss is saved for subsequent evaluation. Further, we use identical hyperparameters for all models during each task.

During pre-training, all models are trained on the same tasks, a mixed set of Poisson, Advection-Diffusion, and Helmholtz equations, comprising a total of  $2^{15} \times 3$  samples. During this stage, we vary the loss function according to the model being trained. The Data-Loss model is trained solely with an  $\mathcal{L}_{\text{data}}$  data loss, the Physics-Loss model is trained with the physics loss term, and the Hybrid-Loss model is trained with both the physics loss term and the data loss term. The Hybrid-Loss model is trained on the same tasks; however, it uses the Missing Solutions dataset (see Appendix B.1). For samples that include solution data, the model incorporates both the physics loss term and the data loss term. However, when the model encounters a sample without a corresponding solution, the data loss term cannot be computed. In such cases, this term is switched off, and only the physics loss is employed.

For downstream tasks, the models are specifically trained on the target PDE dataset using only the  $\mathcal{L}_{\text{data}}$  data loss. The dataset sizes are referred to as Downstream Examples, indicating the number of samples used for training in these tasks. The Scratch model is trained directly on the downstream tasks without any pre-training.

In cases where the downstream tasks do not include coefficients from the pre-training stages, the corresponding coefficient input channels are set to zero. Additionally, if the downstream task introduces new coefficient terms, a zero-shot test is conducted to determine which channel to use for the new coefficient based on the lowest validation loss achieved.

The models are validated and tested on the complete validation and test sets, respectively, using a setup identical to the training of the models.

## C Additional Results

### C.1 Zero-Shot Performance Analysis

In the following, we extend the analysis of zero-shot performance from Section 5.1 and provide additional insights into the models' generalization capabilities across various OOD settings. We evaluate the models on the Poisson, Advection-Diffusion, and Helmholtz tasks, systematically shifting the coefficient ranges OOD. The settings are categorized as follows: ID (in-distribution), Slight-OOD, and High-OOD, as detailed in Table 1. This gradual pushing of the datasets OOD is illustrated in Figure 4 for  $\mu_{\ell_2}$  metric, Figure 5 for  $L_{\infty}$  metric, and Figure 6 for fRMSE metric for models pre-trained with expensive pre-training data and Figure 7, Figure 8 and Figure 9 for models pre-trained on the expanded pre-training set, respectively.

All approaches – Data-Loss, Physics-Loss, and Hybrid-Loss – demonstrate significant improvements in zero-shot generalization, compared to the Scratch model, in both the ID and Slight-OOD settings (see Table 2 and Table 3 and Figures 4, 5, 7 and 8). The results for the Data-Loss approach are consistent with the findings of [22]. At the same time, incorporating Physics-Loss, whether used independently or in combination with Data-Loss, further enhances generalization in these contexts.

The Physics-Loss approach proves particularly effective for the Poisson and Advection-Diffusion ID and Slight-OOD tasks (c.f. Table 2 and Table 3). In contrast, the Hybrid-Loss approach demonstrates greater effectiveness in the Helmholtz setting. This suggests that the loss method based on the PDE residuals is better at capturing the underlying representation of the PDE within the solution space.

In the Helmholtz task, slight changes in the wave number significantly affect the solution space, leading to a more challenging OOD scenario. Under these conditions, the Physics-Loss model's performance deteriorates significantly. Similar trends are observed in the Advection-Diffusion and Poisson tasks when the coefficient ranges are pushed further OOD. This indicates that the Physics-Loss method is sensitive to instances where the solution space diverges considerably from the pre-training data. While the Hybrid-Loss model follows a similar trend, it retains higher performance in High-OOD settings than

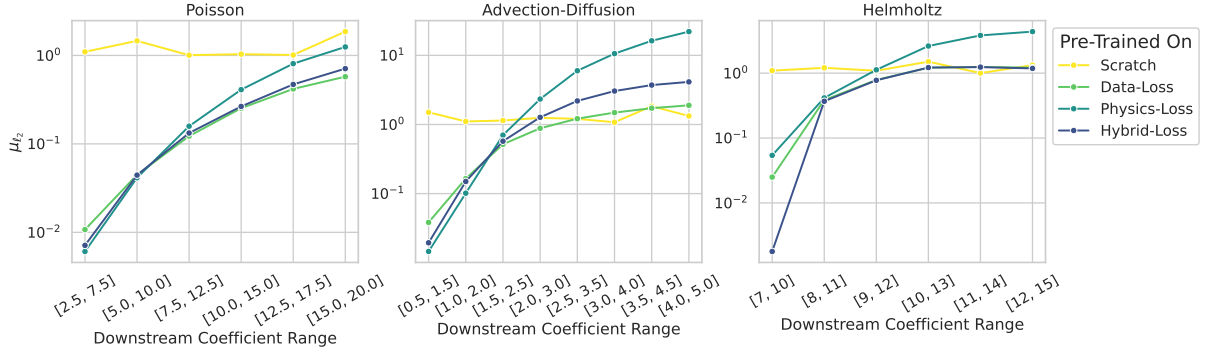


Figure 4: The  $\mu_{\ell_2}$  metric for the downstream tasks of Poisson, Advection-Diffusion, and Helmholtz, respectively, where the coefficient ranges are gradually pushed OOD. The Data-Loss and Hybrid-Loss models are pre-trained on the expensive dataset, while the Physics-Loss model is pre-trained on the synthetic dataset.

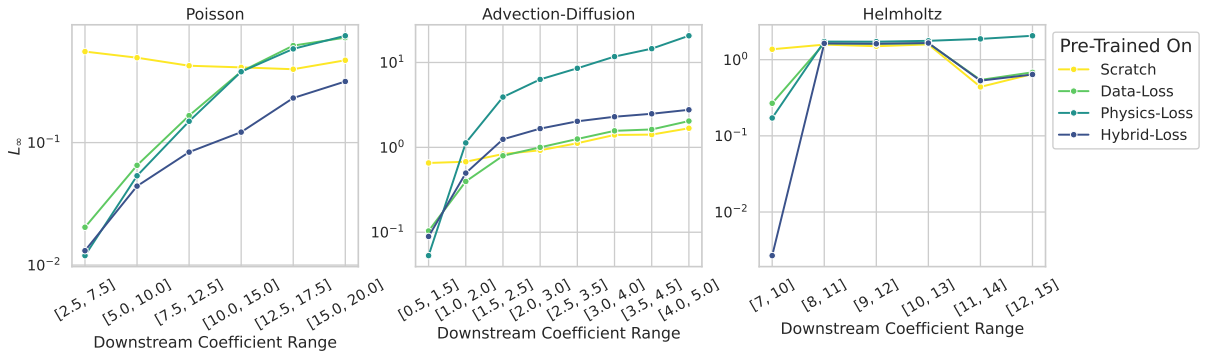


Figure 5: The  $L_{\infty}$  metric for the downstream tasks of Poisson, Advection-Diffusion, and Helmholtz, respectively, where the coefficient ranges are gradually pushed OOD. The Data-Loss and Hybrid-Loss models are pre-trained on the expensive dataset, while the Physics-Loss model is pre-trained on the synthetic dataset.

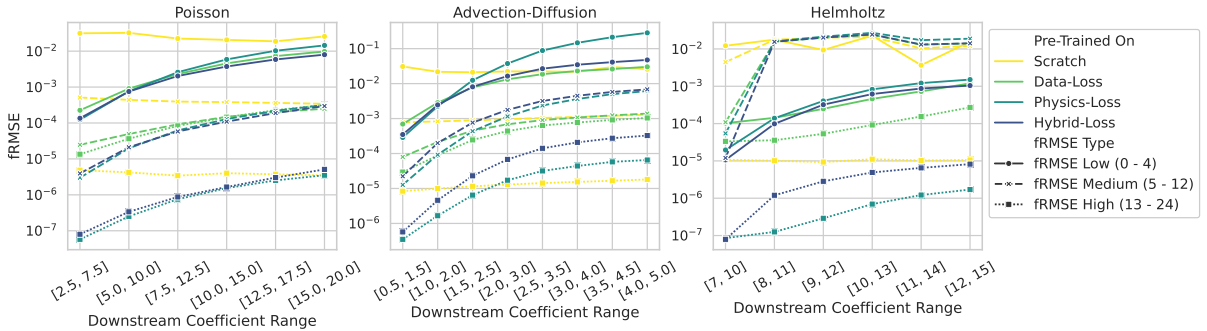


Figure 6: fRMSE metric for the downstream tasks of Poisson, Advection-Diffusion, and Helmholtz, respectively, where the coefficient ranges are gradually pushed OOD. The Data-Loss and Hybrid-Loss models are pre-trained on the expensive dataset, while the Physics-Loss model is pre-trained on the synthetic dataset.

the Physics-Loss model. Meanwhile, the Data-Loss model demonstrates greater robustness to variations in coefficient ranges.

The results for the **Hybrid-Loss** model are of considerable interest. It is important to note that this model is trained on a distinct pre-training dataset, which provides only half the number of samples with solutions for the Poisson and Advection-Diffusion tasks, while no samples with solutions are available for the Helmholtz tasks (see Section B.1). Additionally, the dataset includes samples without solutions, which cannot be used by a model that relies solely on the data loss term. In contrast, the Hybrid-Loss

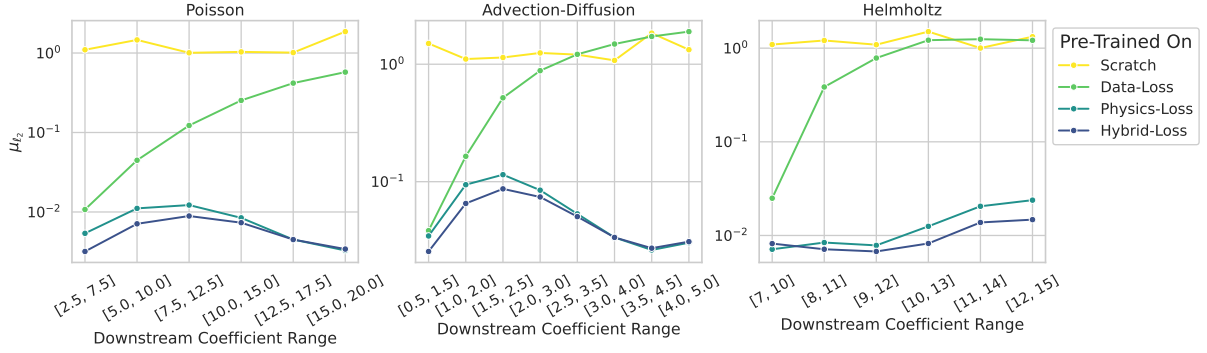


Figure 7: The  $\mu_{\ell_2}$  metric for the downstream tasks of Poisson, Advection-Diffusion, and Helmholtz, respectively, where the coefficient ranges are gradually pushed OOD. While the Physics-Loss and Hybrid-Loss models are pre-trained on the extended pre-training dataset, the Data-Loss model is pre-trained on the expensive dataset.

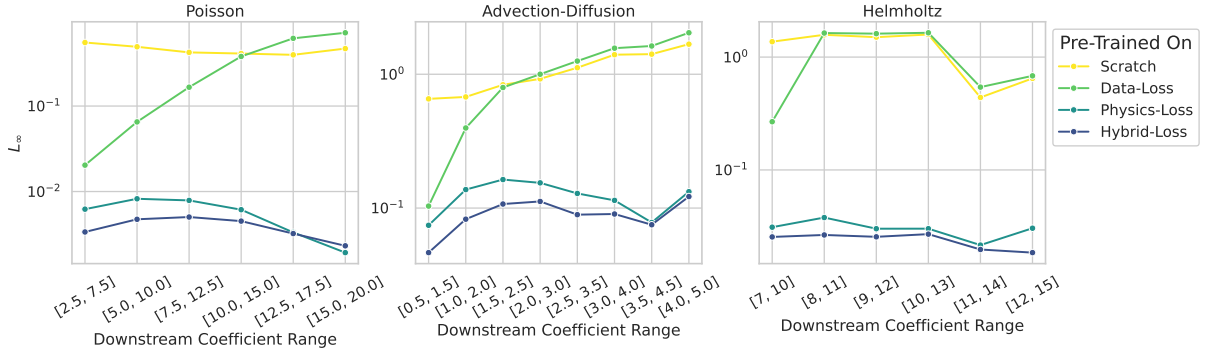


Figure 8: The  $L_{\infty}$  metric for the downstream tasks of Poisson, Advection-Diffusion, and Helmholtz, respectively, where the coefficient ranges are gradually pushed OOD. While the Physics-Loss and Hybrid-Loss models are pre-trained on the extended pre-training dataset, the Data-Loss model is pre-trained on the expensive dataset.

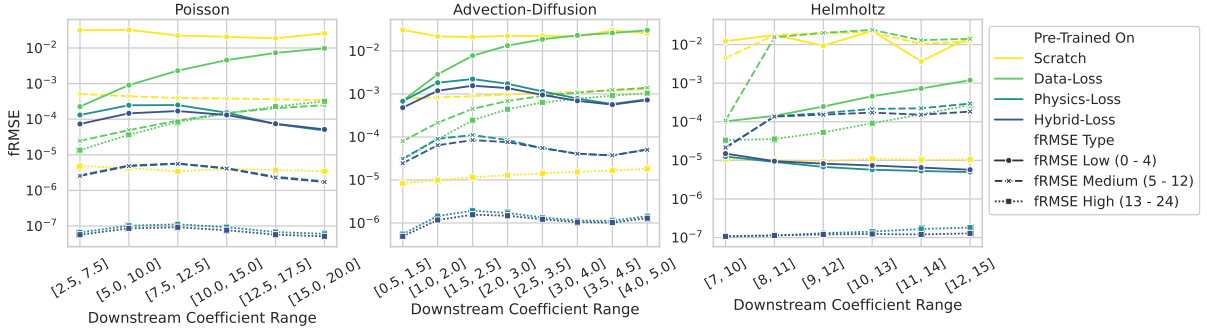


Figure 9: fRMSE metric for the downstream tasks of Poisson, Advection-Diffusion, and Helmholtz, respectively, where the coefficient ranges are gradually pushed OOD. While the Physics-Loss and Hybrid-Loss models are pre-trained on the extended pre-training dataset, the Data-Loss model is pre-trained on the expensive dataset.

model can leverage these samples through the PDE residual term. Using this lower-cost dataset, the Hybrid-Loss model successfully employs the synthetic data to learn a meaningful representation of the underlying systems, as evidenced by its **significantly higher performance** on unseen coefficient ranges. Furthermore, even within the ID datasets, the model demonstrates an ability to outperform the Data-Loss model with significantly fewer samples, thereby highlighting the advantages of enhancing data diversity through low-cost synthetic data.

These results are particularly interesting in the context of the fRMSE metric, which evaluates the model's

performance across various frequency bands in the solution space. The fRMSE metric for the dominant frequency of the target task closely aligns with the  $\mu_{\ell_2}$  and  $L_{\infty}$  metrics, suggesting that the fRMSE metric provides a reliable representation of the model’s performance on downstream tasks (see Figure 6 and Figure 9). We defer a detailed analysis of the fRMSE metric to the n-shot setting in Appendix C.2. The zero-shot baseline results highlight the high sensitivity of the Physics-Loss approach to distribution shifts. Furthermore, they suggest that the data-loss component in the Hybrid-Loss model helps mitigate this sensitivity, improving generalization in downstream tasks.

## C.2 n-Shot Learning Across Various Degrees of Out-of-Distribution

We present an extended analysis of n-shot learning, building on the discussion in Section 5.2. In this analysis, we systematically increase the number of downstream examples used during fine-tuning, ranging from  $2^3$  to  $2^{15}$ , across various coefficient distribution settings categorized as ID (in-distribution), Slight-OOD, and High-OOD, as outlined in Table 1. The results for the Advection-Diffusion and Helmholtz tasks are illustrated in Figures 10 through 21, focusing on the  $\mu_{\ell_2}$ ,  $L_{\infty}$ , and fRMSE metrics, respectively.

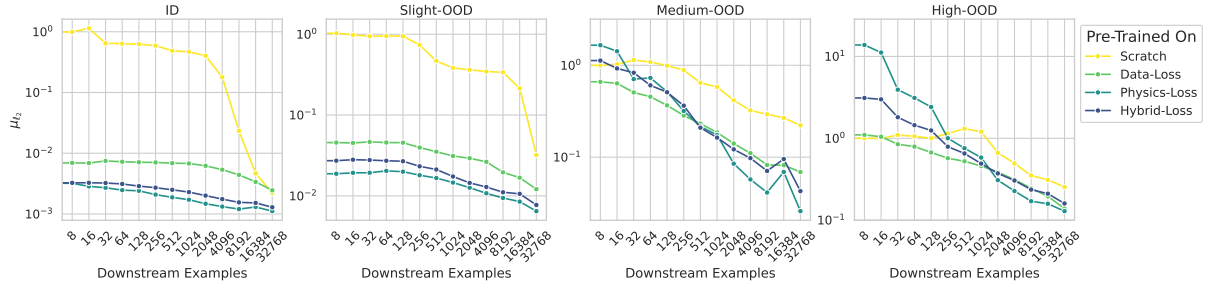


Figure 10:  $\mu_{\ell_2}$  metric for the n-shot target task of Advection-Diffusion is evaluated over an increasing number of downstream examples used during fine-tuning. The overlap with the pre-training data is varied over ID, Slight-OOD, and High-OOD, respectively (c.f. Table 1). The Data-Loss and Hybrid-Loss models are pre-trained on the expensive dataset, while the Physics-Loss model is pre-trained on the synthetic dataset.

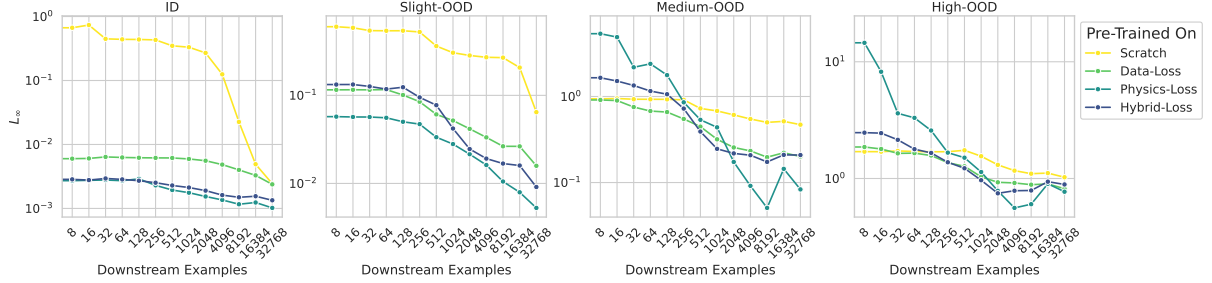


Figure 11:  $L_{\infty}$  metric for the n-shot target task of Advection-Diffusion is evaluated over an increasing number of downstream examples used during fine-tuning. The overlap with the pre-training data is varied over ID, Slight-OOD, and High-OOD, respectively (c.f. Table 1). The Data-Loss and Hybrid-Loss models are pre-trained on the expensive dataset, while the Physics-Loss model is pre-trained on the synthetic dataset.

During the n-shot evaluation, the constraint-aware models for the Advection-Diffusion task exhibit a trend similar to that observed in the zero-shot ID and Slight-OOD settings, even in very low-data scenarios. Furthermore, these models achieve lower  $\mu_{\ell_2}$  and  $L_{\infty}$  metrics compared to the Scratch and the Data-Loss model (c.f. Figure 10, Figure 11, Figure 13 and Figure 14). For the High-OOD setting, where the Physics-Loss model struggled to generalize in the zero-shot context (see Figures 4, 5, 7 and 8), it is able to achieve lower error rates than both baseline models. Further, the Hybrid-Physics Loss model is able to make use of its synthetic data to significantly improve upon the baselines in lower data regimes.

In the ID Helmholtz task, we observe that the performance of the Physics-Loss and Hybrid-Loss models is similar to that in the Advection-Diffusion task, however, flipped (c.f. Figure 16, Figure 17, Figure 19 and Figure 20). The faster improvements in the High-OOD setting can be attributed to the composition

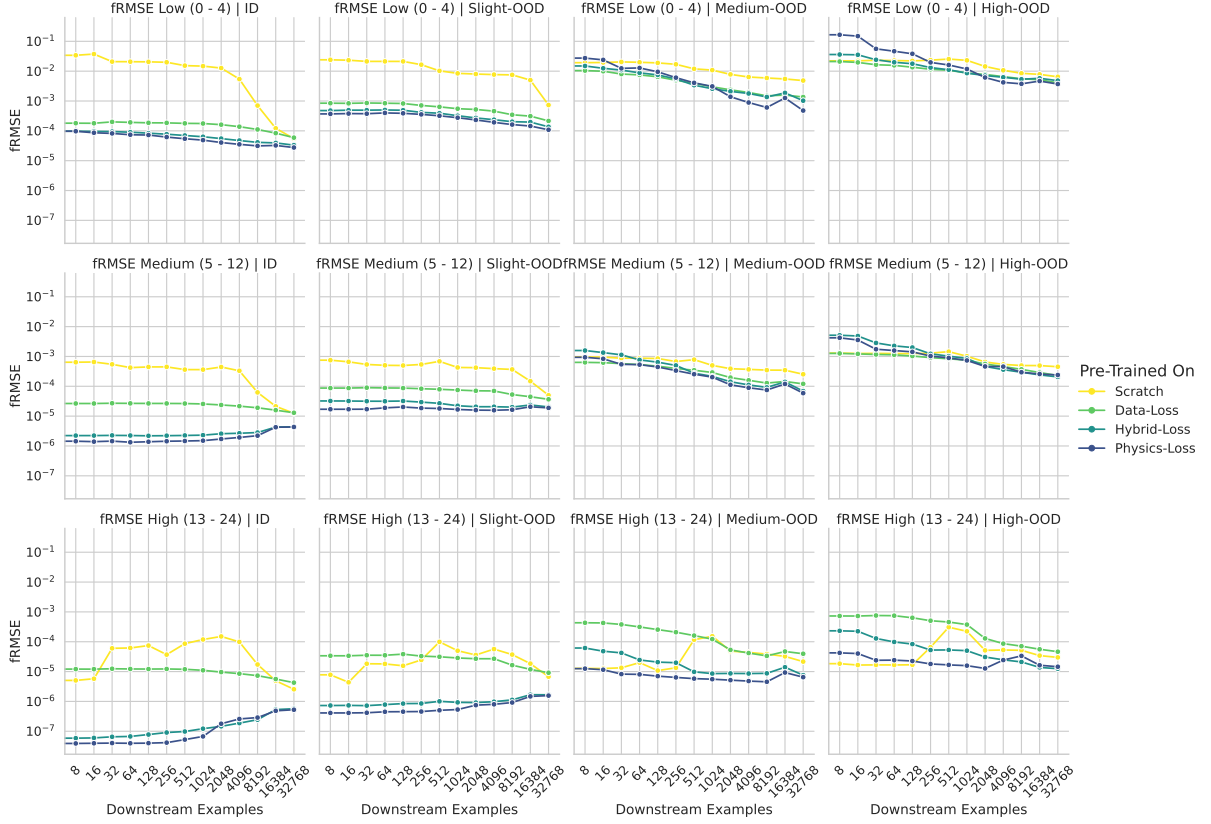


Figure 12: fRMSE metric for the n-shot target task of Advection-Diffusion is evaluated over an increasing number of downstream examples used during fine-tuning. The Data-Loss and Hybrid-Loss models are pre-trained on the expensive dataset, while the Physics-Loss model is pre-trained on the synthetic dataset.

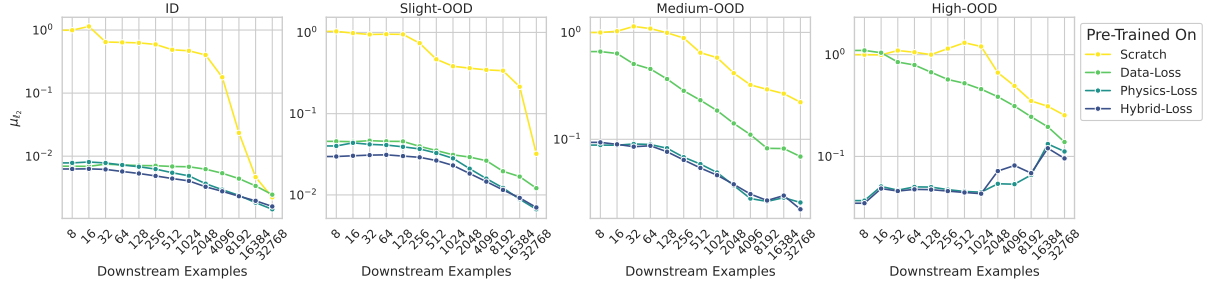


Figure 13:  $\mu_{\ell_2}$  metric for the n-shot target task of Advection-Diffusion is evaluated over an increasing number of downstream examples used during fine-tuning. The overlap with the pre-training data is varied over ID, Slight-OOD, and High-OOD, respectively (c.f. Table 1). While the Physics-Loss and Hybrid-Loss models are pre-trained on the extended pre-training dataset, the Data-Loss model is pre-trained on the expensive dataset.

of the OOD dataset, which, in contrast to the Slight-OOD setting, consists solely of OOD samples. As a result, all samples are beneficial for adapting the model to the OOD context. In both the Slight-OOD and High-OOD settings, the Hybrid-Loss model achieves significantly lower  $\mu_{\ell_2}$  and  $L_{\infty}$  metrics in higher data regimes compared to other models, while for low data regimes the Hybrid-Loss model again significantly improves upon the baselines in lower data regimes.

The results show that the Physics-Loss and Hybrid-Loss models exhibit strong generalization in the Advection-Diffusion and Helmholtz tasks, even under higher OOD conditions. However, consistent with the zero-shot setting, the Physics-Loss model remains highly sensitive to significant changes in the solution space, as observed in the results of the Helmholtz task.

The data-loss term in the Hybrid-Loss model effectively mitigates this sensitivity while retaining the benefits of the Physics-Loss approach. Furthermore, models incorporating Physics-Loss during pre-training

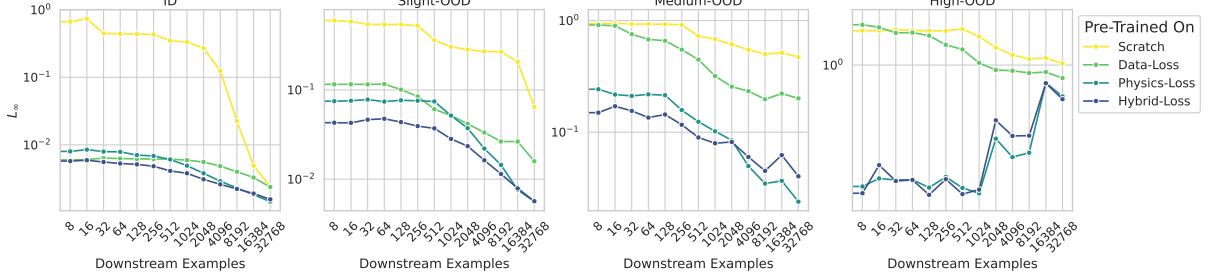


Figure 14:  $L_\infty$  metric for the n-shot target task of Advection-Diffusion is evaluated over an increasing number of downstream examples used during fine-tuning. The overlap with the pre-training data is varied over ID, Slight-OOD, and High-OOD, respectively (c.f. Table 1). While the Physics-Loss and Hybrid-Loss models are pre-trained on the extended pre-training dataset, the Data-Loss model is pre-trained on the expensive dataset.

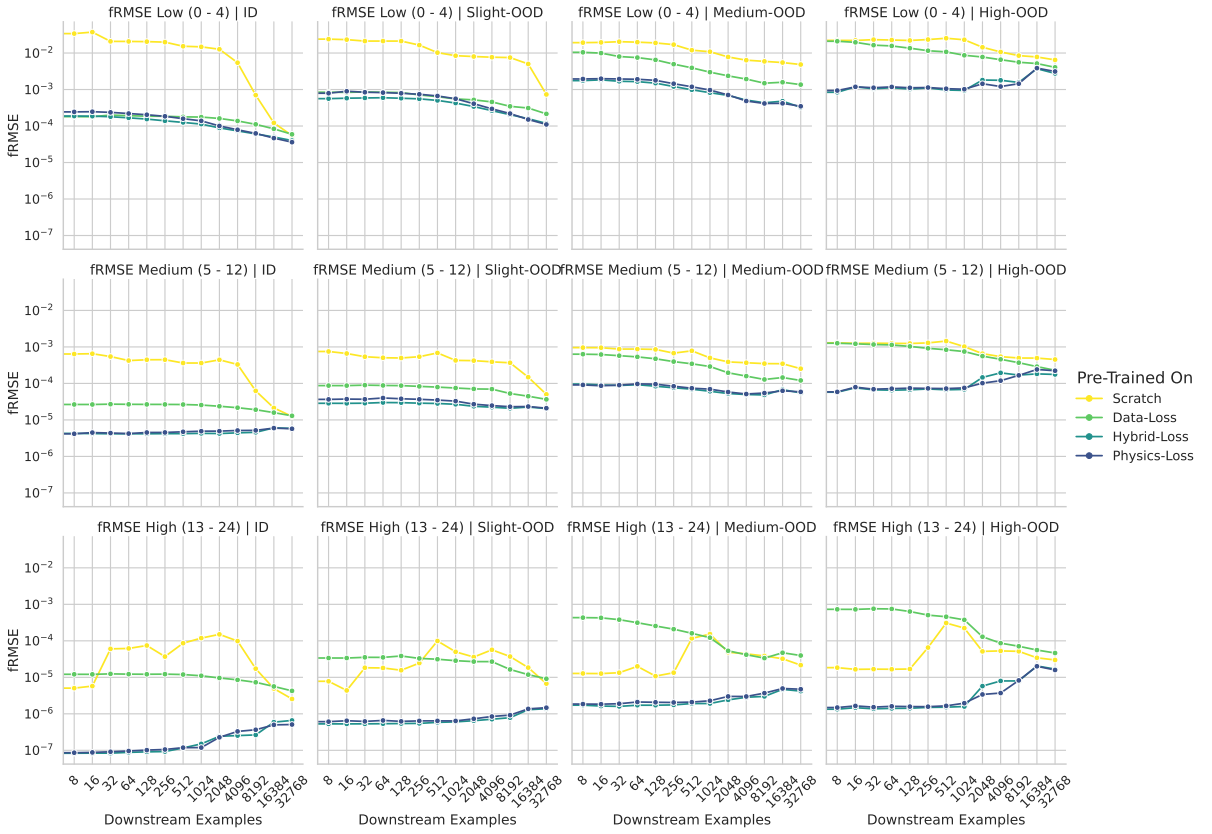


Figure 15: fRMSE metric for the n-shot target task of Advection-Diffusion is evaluated over an increasing number of downstream examples used during fine-tuning. While the Physics-Loss and Hybrid-Loss models are pre-trained on the extended pre-training dataset, the Data-Loss model is pre-trained on the expensive dataset.

achieve lower error rates compared to models trained from scratch.

The Hybrid-Loss model consistently demonstrates robust generalization in lower data regimes across all tasks. However, in higher data regimes of OOD datasets, we observe a decline in performance, approaching levels comparable to zero-shot performance. This reduction in performance is also reflected in the model’s training loss, which exhibits a magnitude difference of an order of ten when compared to lower data regimes. This suggests that the 500 epochs may be insufficient for the model to achieve convergence in higher data regimes. The lack of sufficient convergence may stem from a transition from a predominantly PDE residual-defined loss landscape to a data loss-dominated landscape in higher OOD scenarios. This shift, coupled with the amount of data, may significantly complicate the convergence process within the loss landscape, resulting in extended convergence times during training.

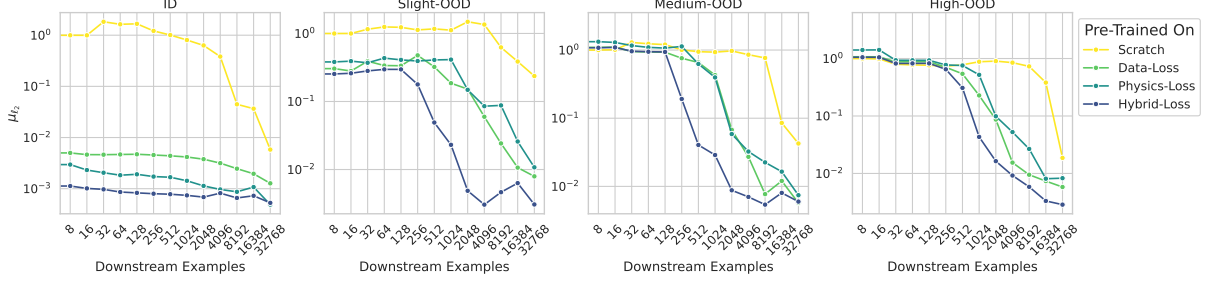


Figure 16:  $\mu_{\ell_2}$  metric for the n-shot target task of Helmholtz is evaluated over an increasing number of downstream examples used during fine-tuning. The overlap with the pre-training data is varied over ID, Slight-OOD, and High-OOD, respectively (c.f. Table 1). The Data-Loss and Hybrid-Loss models are pre-trained on the expensive dataset, while the Physics-Loss model is pre-trained on the synthetic dataset.

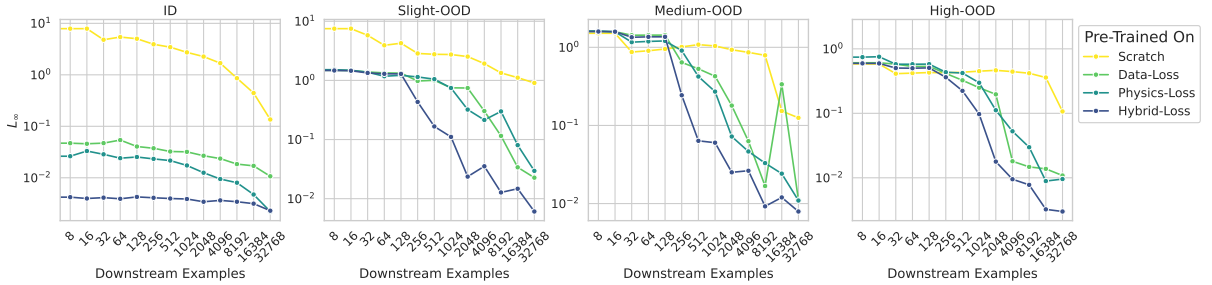


Figure 17:  $L_{\infty}$  metric for the n-shot target task of Helmholtz is evaluated over an increasing number of downstream examples used during fine-tuning. The overlap with the pre-training data is varied over ID, Slight-OOD, and High-OOD, respectively (c.f. Table 1). The Data-Loss and Hybrid-Loss models are pre-trained on the expensive dataset, while the Physics-Loss model is pre-trained on the synthetic dataset.

Under the zero-shot setting, we observed a correlation between the fRMSE metric and the  $\mu_{\ell_2}$  and  $L_{\infty}$  metrics for the dominant frequency of the target task, suggesting that the fRMSE metric provides a reliable representation of the model’s performance on downstream tasks (see Figure 6 and Figure 9). This correlation is also evident in the n-shot tasks of the Advection-Diffusion and Helmholtz systems.

In the n-shot Advection-Diffusion task, the fRMSE metric for lower frequencies closely aligns with the  $\mu_{\ell_2}$  and  $L_{\infty}$  metrics (c.f. Figure 12 and Figure 15, and Figures 10, 11, 13 and 14 respectively). In contrast, for the Helmholtz task, the fRMSE metric for medium to high frequencies serves as a better indicator of the model’s performance (c.f. Figures 18, 16, 17 for the models pre-trained on the expensive dataset and respectively Figures 21, 19, 20 on the extended).

Therefore, the problem can be framed as one of predicting the frequencies present in the target system’s solution space. Under this assumption, the performance improvements of models augmented with Physics-Loss can be attributed to a better representation of the underlying frequencies in the solution space, as the Physics-Loss term implicitly guides the minimization of frequency error through the constraints imposed by the PDE.

However, the frequency domain of a target system might change significantly with changes to the coefficient ranges, as observed in the Helmholtz task. These changes significantly impact the Physics-Loss model’s initial performance. However, the Data-Loss term lacks this implicit guidance, which may explain the better performance of the Hybrid-Loss. This term may mitigate this sensitivity to changes in the solution space while retaining the advantages of the Physics-Loss approach.

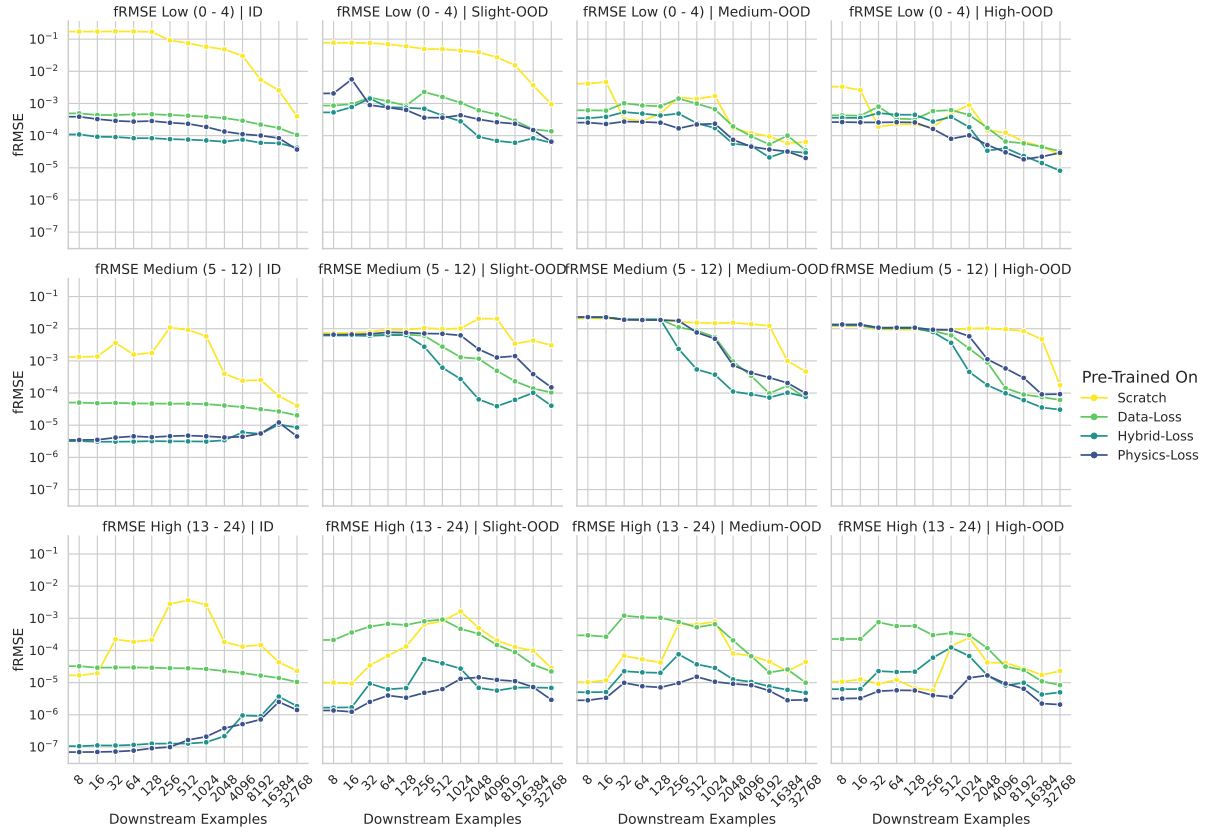


Figure 18: fRMSE metric for the n-shot target task of Helmholtz is evaluated over an increasing number of downstream examples used during fine-tuning. The Data-Loss and Hybrid-Loss models are pre-trained on the expensive dataset, while the Physics-Loss model is pre-trained on the synthetic dataset.

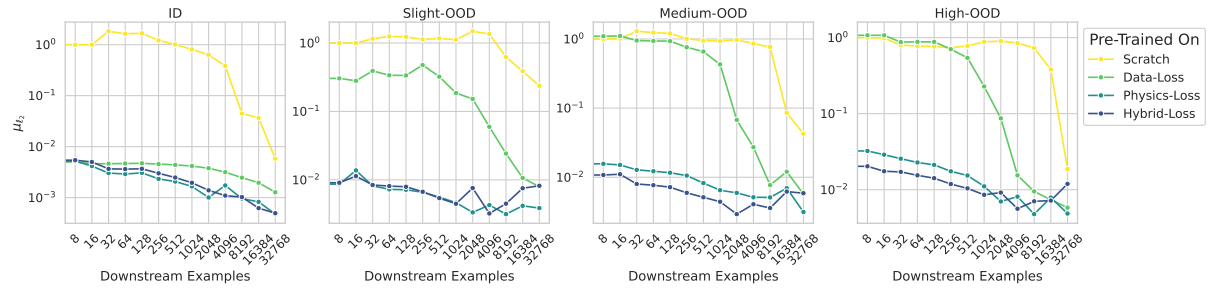


Figure 19:  $\mu_{\ell_2}$  metric for the n-shot target task of Helmholtz is evaluated over an increasing number of downstream examples used during fine-tuning. The overlap with the pre-training data is varied over ID, Slight-OOD, and High-OOD, respectively (c.f. Table 1). While the Physics-Loss and Hybrid-Loss models are pre-trained on the extended pre-training dataset, the Data-Loss model is pre-trained on the expensive dataset.

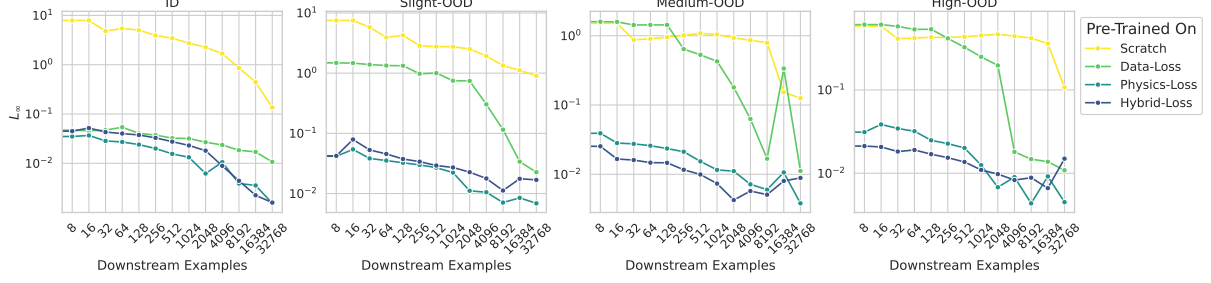


Figure 20:  $L_\infty$  metric for the n-shot target task of Helmholtz is evaluated over an increasing number of downstream examples used during fine-tuning. The overlap with the pre-training data is varied over ID, Slight-OOD, and High-OOD, respectively (c.f. Table 1). While the Physics-Loss and Hybrid-Loss models are pre-trained on the extended pre-training dataset, the Data-Loss model is pre-trained on the expensive dataset.

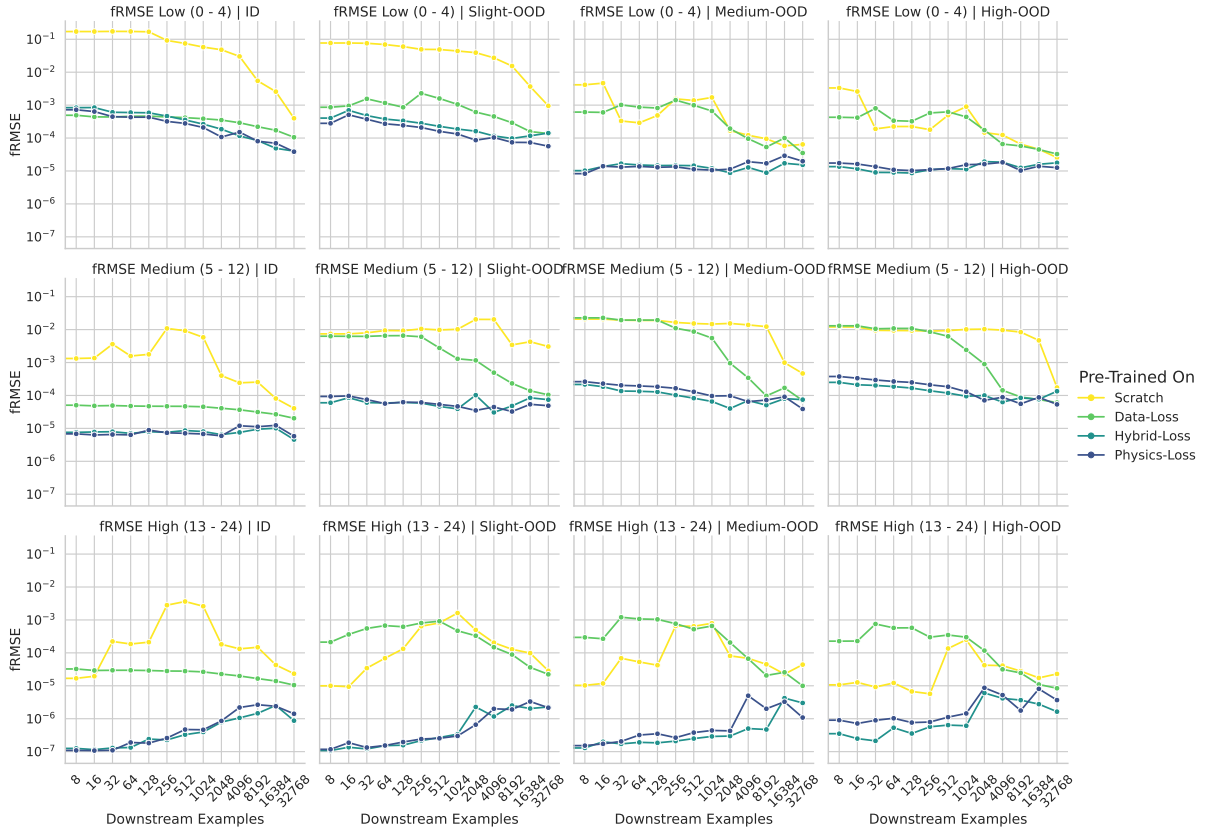


Figure 21: fRMSE metric for the n-shot target task of Helmholtz is evaluated over an increasing number of downstream examples used during fine-tuning. While the Physics-Loss and Hybrid-Loss models are pre-trained on the extended pre-training dataset, the Data-Loss model is pre-trained on the expensive dataset.

### C.3 n-Shot with Noisy Solution Space

Here, we extend the analysis of model performance for the n-shot learning setting under different degrees of noise in the solution space. We evaluate the models on the Advection-Diffusion and Helmholtz tasks, systematically increasing the noise level from  $\sigma = 0.01$  to  $\sigma = 0.2$ . The results are categorized as ID (in-distribution), Slight-OOD, and High-OOD, as outlined in Table 1. The results for the  $\mu_{\ell_2}$ ,  $L_{\infty}$ , and fRMSE metrics are illustrated in Figures 22 through 28, additionally to Figure 2 from Section 5.2.

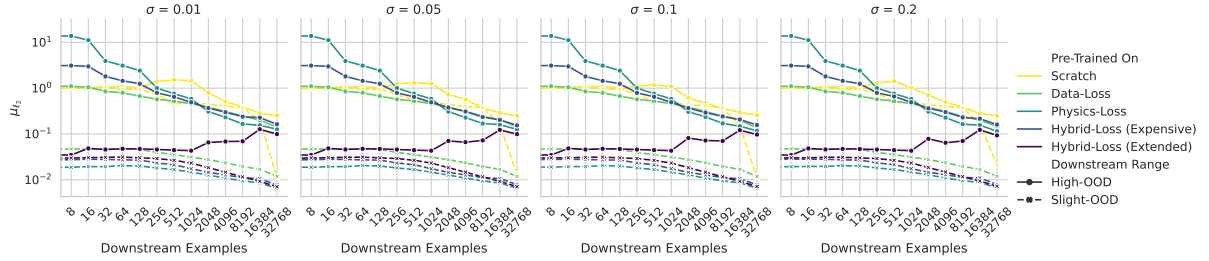


Figure 22: Evaluation of the  $\mu_{\ell_2}$  metric for varying degrees of noise in the solution domain for the OOD pushed datasets in the Advection-Diffusion task. From left to right,  $\sigma$  takes the form of 0.01, 0.05, 0.1, and 0.2.

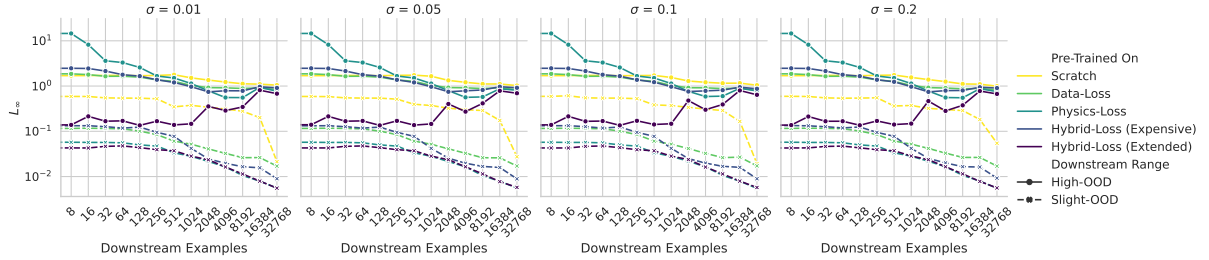


Figure 23: Evaluation of the  $L_{\infty}$  metric for varying degrees of noise in the solution domain for the OOD pushed datasets in the Advection-Diffusion task. From left to right,  $\sigma$  takes the form of 0.01, 0.05, 0.1, and 0.2.

Comparing the results of the Advection-Diffusion and Helmholtz tasks, illustrated in Figure 22 and Figure 2, we find that constrained-aware models are not significantly impacted by noise in the solution space, as measured by the  $\mu_{\ell_2}$  metric. A similar trend is observed in the  $L_{\infty}$  metric, illustrated in Figures 23 and 26.

Moreover, the constrained-aware models consistently outperform the baseline models across all noise levels, achieving error rates comparable to those observed in the noise-free setting for both the Advection-Diffusion task (see Figure 10 and Figure 13) and the Helmholtz task (see Figure 16 and Figure 19).

This trend indicates that the constraint-aware models are adept at capturing solution components across various scales, even in the presence of noise. Given that Additive White Gaussian Noise (AWGN) is a high-frequency signal, the fRMSE metric for higher frequencies offers a more accurate assessment of the model's performance under noisy conditions. The fRMSE metrics for the Advection-Diffusion and Helmholtz tasks, presented in Figures 24 and 27 for the Slight-OOD setting, and Figures 25 and 28 for the High-OOD setting, reveal that neither of the constrained-aware models is significantly affected by noise in the solution space when compared to their fRMSE performance in the noise-free setting (see Figure 15 and Figure 12 for Advection-Diffusion and Figure 21 and Figure 18). This further confirms the robustness of the models against noise in the solution space.

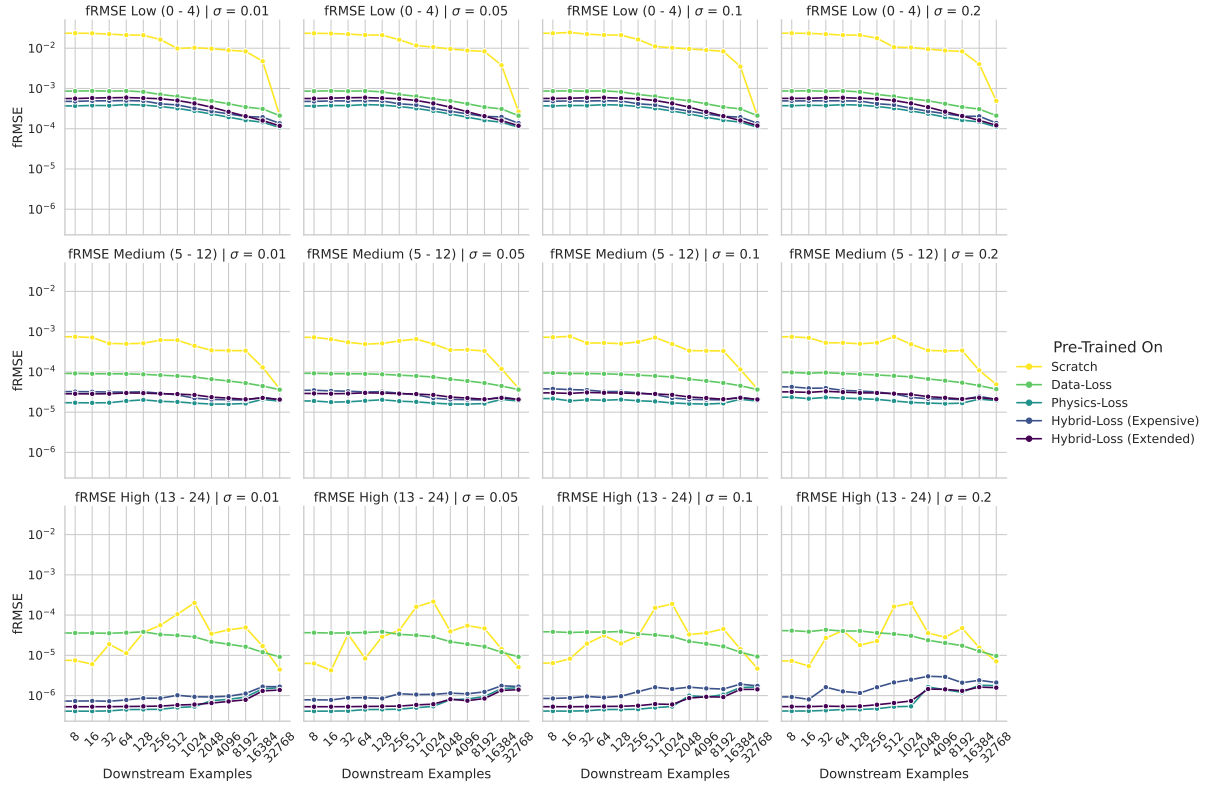


Figure 24: Evaluation of the fRMSE metric for varying degrees of noise in the solution domain for Advection-Diffusion Slight-OOD task.

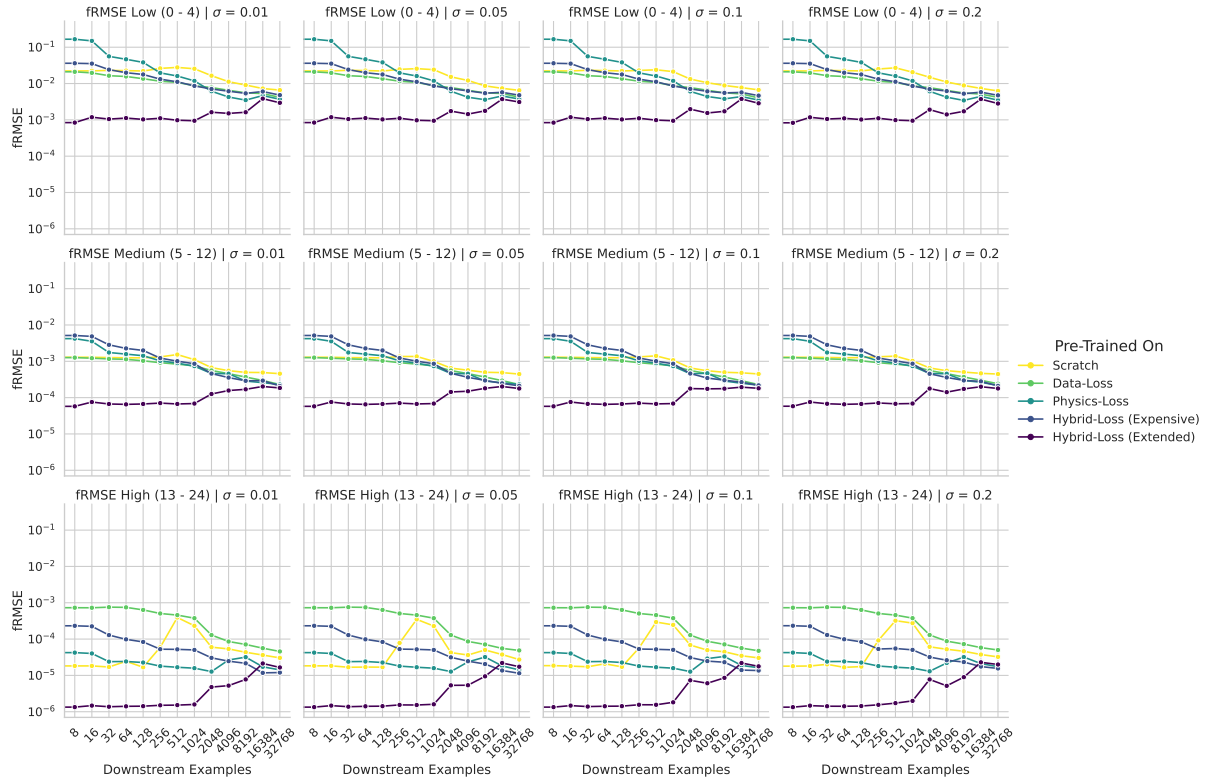


Figure 25: Evaluation of the fRMSE metric for varying degrees of noise in the solution domain for Advection-Diffusion High-OOD task.

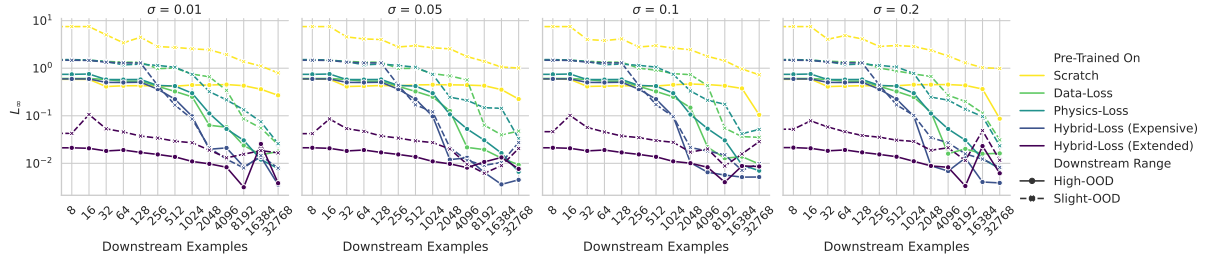


Figure 26: Evaluation of the  $L_\infty$  metric for varying degrees of noise in the solution domain for the OOD pushed datasets in the Helmholtz task. From left to right,  $\sigma$  takes the form of 0.01, 0.05, 0.1, and 0.2.

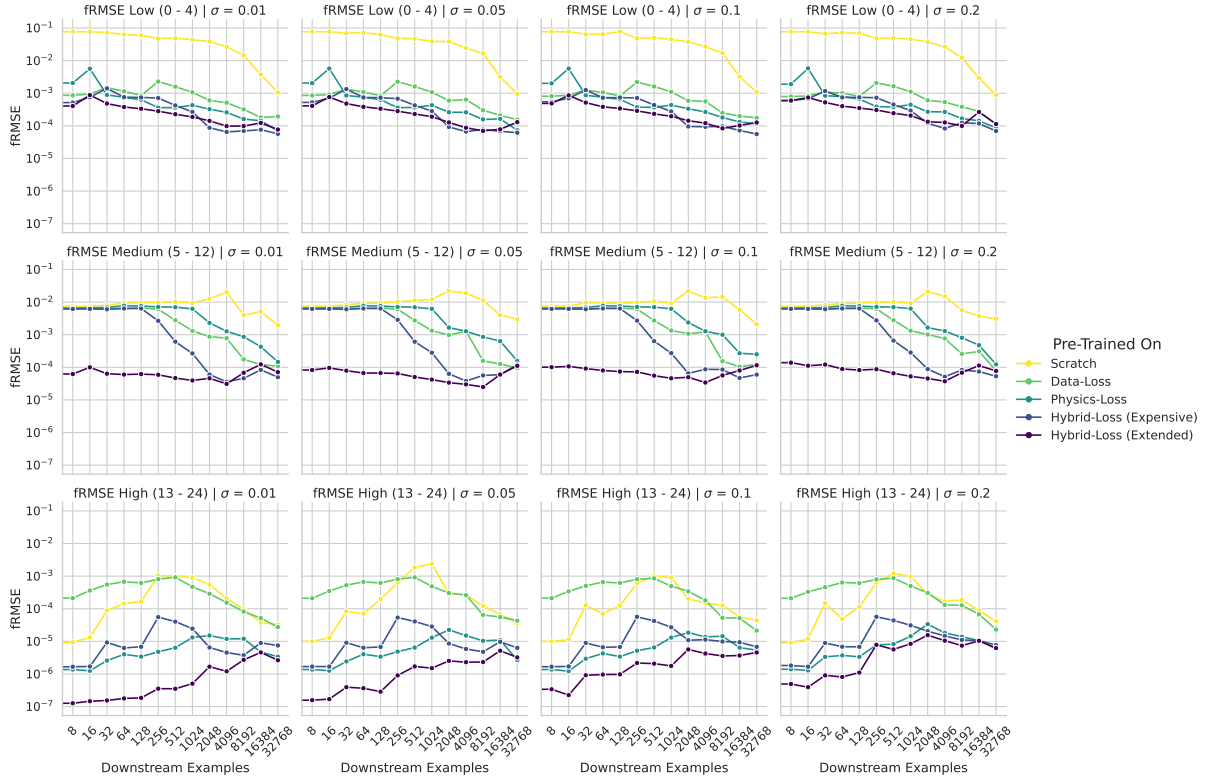


Figure 27: Evaluation of the fRMSE metric for varying degrees of noise in the solution domain for Helmholtz Slight-OOD task.

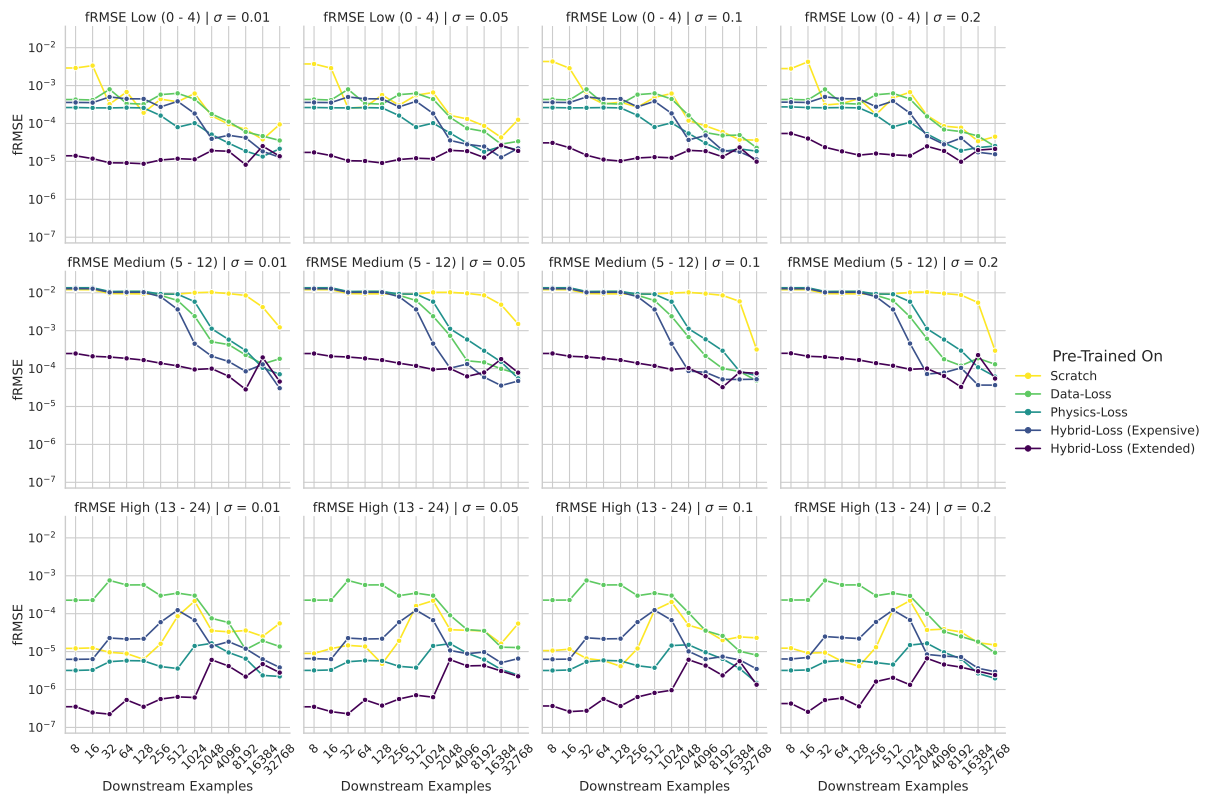


Figure 28: Evaluation of the fRMSE metric for varying degrees of noise in the solution domain for Helmholtz High-OOD task.

## C.4 Shifting Focus to Unseen PDEs

We present the  $L_\infty$  metric for the Darcy, Reaction-Diffusion, and Reaction-Advection-Diffusion tasks in Figure 29 and Figure 30, alongside fRMSE results in Figure 31 and Figure 32 for models pre-trained on expensive and extended datasets. These systems represent a significant departure from the pre-training tasks as they introduce new physics and dynamics. Note that these PDEs were not used during pre-training stage.

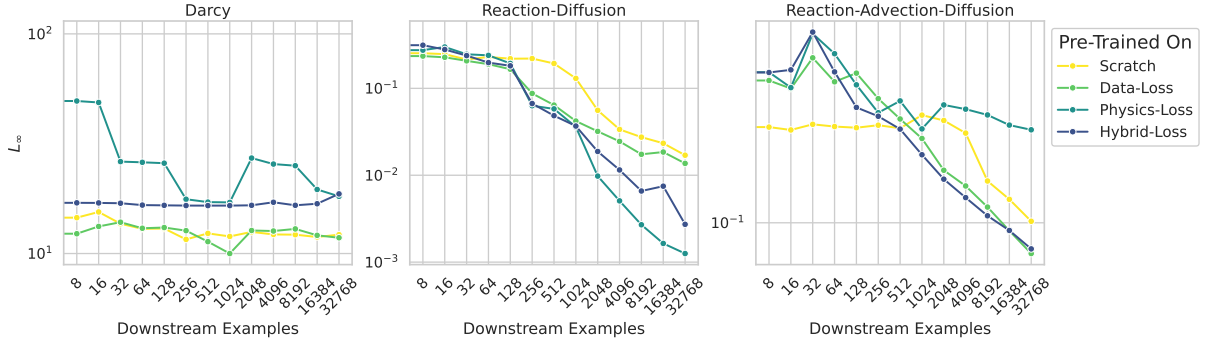


Figure 29: The  $L_\infty$  metrics for the downstream tasks of Darcy, Reaction-Diffusion, and Reaction-Advection-Diffusion, respectively, with an increasing number of downstream examples used during fine-tuning. The Data-Loss and Hybrid-Loss models are pre-trained on the expensive dataset, while the Physics-Loss model is pre-trained on the synthetic dataset.

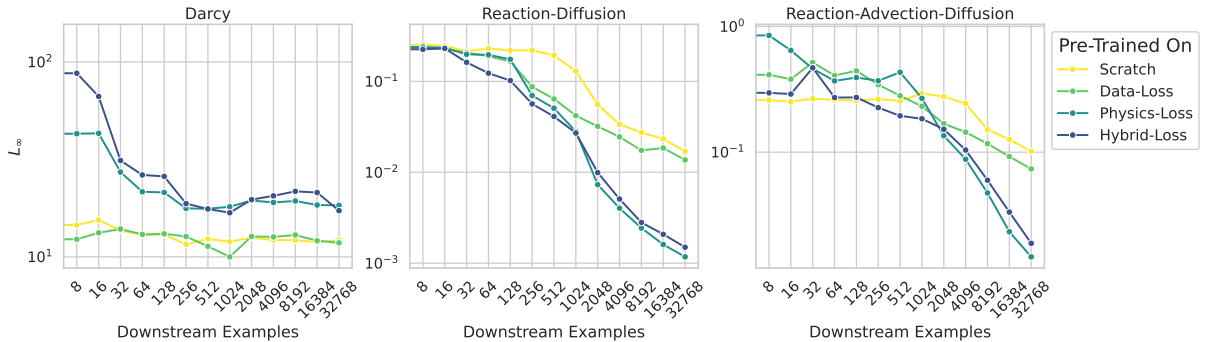


Figure 30: The  $L_\infty$  metrics for the downstream tasks of Darcy, Reaction-Diffusion, and Reaction-Advection-Diffusion, respectively, with an increasing number of downstream examples used during fine-tuning. While the Physics-Loss and Hybrid-Loss models are pre-trained on the extended pre-training dataset, the Data-Loss model is pre-trained on the expensive dataset.

The analysis of the Darcy task focuses on fluid flow through porous media, characterized by the coefficient tensor  $\mathbf{K}$ . This tensor governs the medium's resistance to flow and differs significantly from the coefficients used in the pre-training tasks, as it is not a scalar value but rather a function of the spatial domain. In addition to this change, the Darcy task introduces Dirichlet boundary conditions, marking a notable departure from the periodic boundary conditions employed in the pre-training tasks.

In alignment with the results for the  $\mu_{\ell_2}$  metric, as depicted in Figure 3, the  $L_\infty$  metric results for the Darcy task (see Figures 29 and 30) indicate that no model achieves a significant reduction in errors, even with a substantial number of downstream examples. In contrast to the  $\mu_{\ell_2}$  metric, the Hybrid-Loss model demonstrates a higher  $L_\infty$  error, comparable to that of the Physics-Loss model. This elevated error rate is also evident in the dominant frequency ranges, as illustrated in Figure 29 and Figure 30.

For the Reaction-Diffusion task, the  $L_\infty$  metric (see Figure 29 and Figure 30), like the  $\mu_{\ell_2}$  metric, demonstrates a significant reduction in error for the constrained-aware models compared to the baseline models. Additionally, the fRMSE results (see Figure 31 and Figure 32) indicate that the constrained-aware models effectively reduce errors across all frequency ranges, with the most notable improvements occurring in the lower frequencies, which are predominant in the Reaction-Diffusion task. This trend is consistent with the results observed in the zero-shot and n-shot settings.



Figure 31: fRMSE metrics for the downstream tasks of Darcy, Reaction-Diffusion, and Reaction-Advection-Diffusion, with an increasing number of downstream examples used during fine-tuning. The Data-Loss and Hybrid-Loss models are pre-trained on the expensive dataset, while the Physics-Loss model is pre-trained on the synthetic dataset.

The Reaction-Advection-Diffusion task integrates the effects of advection, diffusion, and reaction processes commonly encountered in environmental and industrial applications. In addition to the scalar reaction term from the Reaction-Diffusion task, the advection term introduces a vector function of the solution space, which captures the transport of species influenced by the velocity field, potentially leading to significant shifts in the solution space.

This shift is evident in the results, where we observe trends similar to those seen in the Helmholtz task (see Figure 16 and Figure 19 for  $\mu_{\ell_2}$  and Figure 17 and Figure 20 for  $L_{\infty}$ ), as well as in the higher OOD setting of the Advection-Diffusion task (see Figure 10 and Figure 13 for  $\mu_{\ell_2}$  and Figure 11 and Figure 14 for  $L_{\infty}$ ), where the constraint-aware models struggle to reduce the error significantly over the baseline model and the Physics-Loss model fails. This further highlights the sensitivity of the Physics-Loss model to variations in the solution space, which is consistent with the findings from both the zero-shot and n-shot analyses.

The results for the Reaction-Diffusion task can be attributed to its structural similarity with the pre-training PDEs, particularly the Poisson and Advection-Diffusion equations. In contrast, the Darcy task introduces a significant change in boundary conditions, shifting from periodic to Dirichlet boundary conditions. This transition presents inherent challenges for FNO architectures, underscoring a fundamental limitation of this approach in managing certain types of boundary conditions.

However, the higher error rates observed in the Reaction-Advection-Diffusion and Darcy tasks for

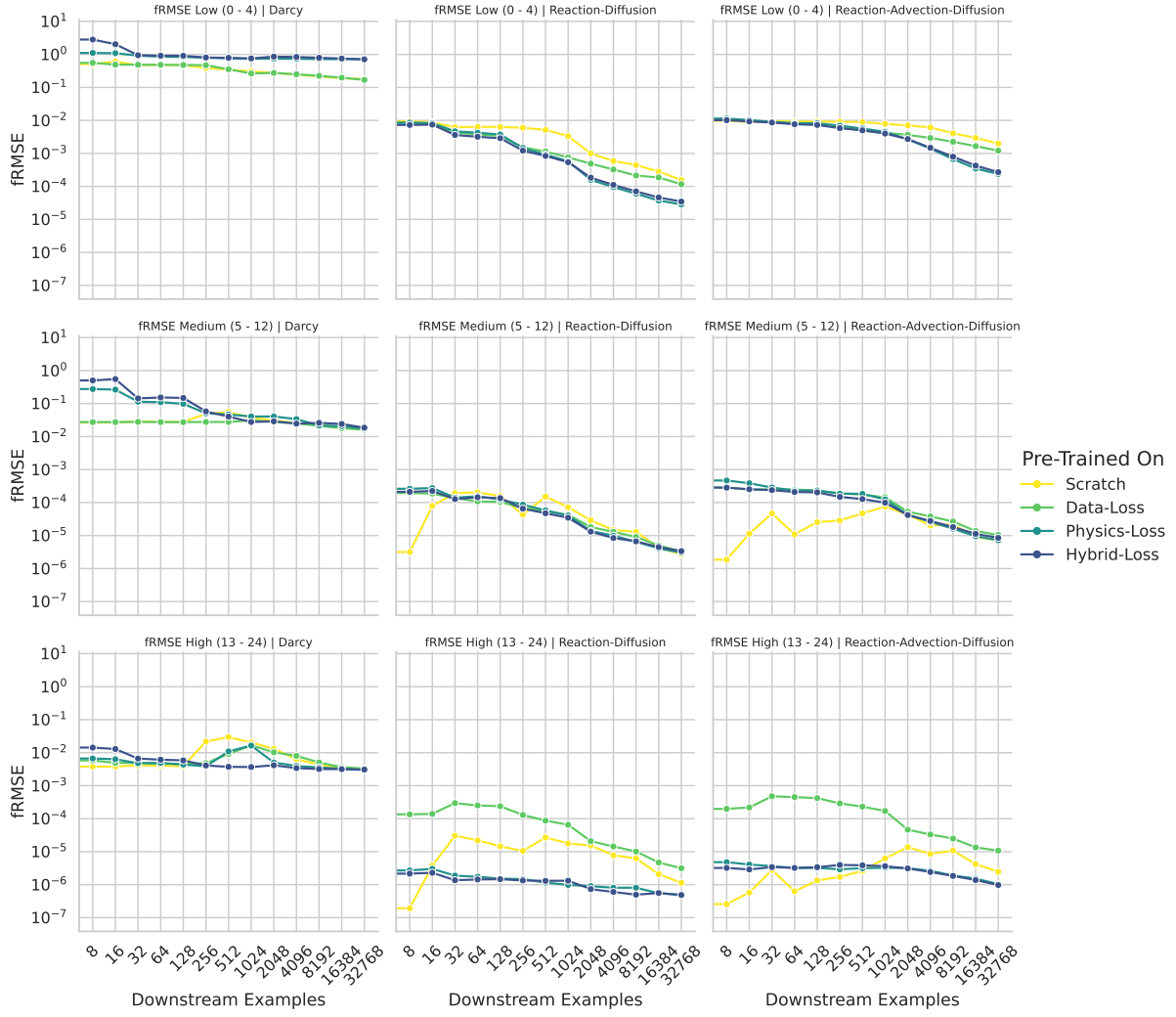


Figure 32: fRMSE metrics for the downstream tasks of Darcy, Reaction-Diffusion, and Reaction-Advection-Diffusion, with an increasing number of downstream examples used during fine-tuning. While the Physics-Loss and Hybrid-Loss models are pre-trained on the extended pre-training dataset, the Data-Loss model is pre-trained on the expensive dataset.

the Physics-Loss model indicate that constraint-aware training does not transfer effectively to tasks characterized by significant shifts in the solution space. This limitation is particularly evident in the dominant frequency ranges, as highlighted by the fRMSE results, and is consistent with the findings from both the zero-shot and n-shot settings. This trend may suggest that the Physics-Loss model overfits the pre-training tasks, resulting in a lack of generalization to new systems with significantly different dynamics.

In contrast, the Hybrid-Loss model exhibits similar robustness to shifts in the Reaction-Advection-Diffusion task as seen in the Helmholtz task, indicating that the data-loss term effectively mitigates the model’s sensitivity to changes in the solution space. Considering the Hybrid-Loss model trained on the extended dataset improvements in performance over the Physics-Loss, it highlights how important a diverse dataset becomes for the transferability capacity of a model to other domains.